

Interactive Exploration of Physically-Observable Objective Vortices in Unsteady 2D Flow

Xingdi Zhang, Markus Hadwiger, Thomas Theußl, Peter Rautek

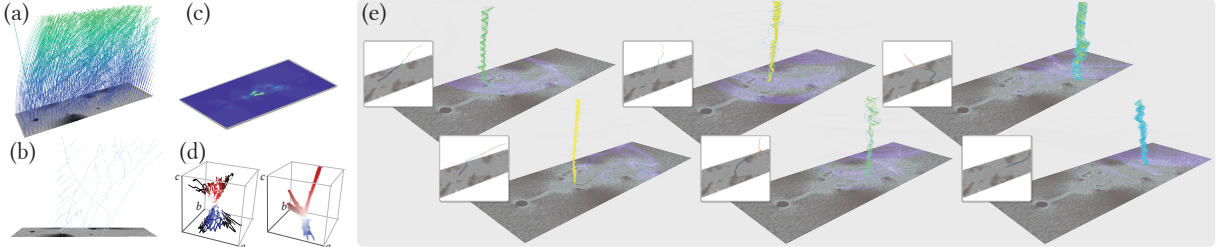


Fig. 1. **Vortex structures** (b; λ_2 vortex cores) not visible in the input flow (a) become visible relative to different observers (e). (Vertical axis is time.) Because all observers (six observers in insets) were computed using objective optimization, the observed vortices are also objective. However, each observer is also physically realizable. This guarantees that these vortices are also physically observable. We represent observers as curves through the Lie algebra of physically-realizable observer motions, which is a special 3D vector space. Choosing a basis defines an (a, b, c) parameter space (d), enabling efficient averaging, interpolation, and comparison of observers (c).

Abstract—State-of-the-art computation and visualization of vortices in unsteady fluid flow employ objective vortex criteria, which makes them independent of reference frames or observers. However, objectivity by itself, although crucial, is not sufficient to guarantee that one can identify physically-realizable observers that would perceive or detect the same vortices. Moreover, a significant challenge is that a single reference frame is often not sufficient to accurately observe multiple vortices that follow different motions. This paper presents a novel framework for the exploration and use of an interactively-chosen set of observers, of the resulting relative velocity fields, and of objective vortex structures. We show that our approach facilitates the objective detection and visualization of vortices relative to well-adapted reference frame motions, while at the same time guaranteeing that these observers are in fact physically realizable. In order to represent and manipulate observers efficiently, we make use of the low-dimensional vector space structure of the Lie algebra of physically-realizable observer motions. We illustrate that our framework facilitates the efficient choice and guided exploration of objective vortices in unsteady 2D flow, on planar as well as on spherical domains, using well-adapted reference frames.

Index Terms—Flow visualization, vortex detection, objectivity, observers, reference frames, Lie algebras

1 INTRODUCTION

A significant amount of recent research in flow visualization and continuum mechanics has built on the concept of objectivity [14, 17, 19, 39]. For vortex detection, for instance, it is crucial that the employed criteria are objective, because otherwise different observers can come to different conclusions on where vortices are located. For this reason, non-objective criteria often might not correspond to physical reality. However, even objectivity, by itself, only guarantees that different observers reach the same conclusions, but not necessarily how physically-plausible these conclusions are. In particular, it is known that for many real-world flow phenomena a single reference frame is not sufficient in order to detect or depict all features of interest [14, 29]. For this reason, generic objective approaches have been proposed that use a large number of observers and detect features jointly [4, 14, 18, 39]. These approaches, however, focus on overall objectivity, and not on confirming that each detected feature would in fact be able to be perceived by a physically-realizable observer. In this paper, we therefore target the additional consideration whether *some*, a priori unknown, but

physically-realizable, observer is able to reach the same conclusion.

We propose to address the gap between using a single, physically-realizable observer on the one hand, and joint methods using many observers on the other hand, via an interactive framework for 2D unsteady flow that (1) employs only physically-realizable observers; and (2) enables users to explore arbitrary sets of observers together with the flow phenomena they perceive, in order to ultimately determine a set of observers that is sufficient to detect and visualize all structures of interest. A crucial property of our framework is that we enable interactively choosing, averaging, and interpolating observers, coupled with interactive observer-relative visualization and feature detection.

1.1 Mathematical Framework

Before introducing our framework, we first briefly introduce several crucial concepts that are not standard in the flow visualization literature. We refer to later sections as well as the appendixes in the supplementary material for details and more background on these concepts.

Physically-realizable observers. We call a reference frame that is described by a time-dependent rigid motion a *physically-realizable observer*, since every reference frame motion that can be carried out in reality must preserve Euclidean distances [46] (neglecting relativistic effects). The most important consequence of this fact in our context is that we can thus model all such observers by vector fields that are the derivatives of rigid motions, obtaining the motion via integration.

Killing vector fields. The derivatives of rigid motions are given by Killing vector fields [32, 38], corresponding to the *infinitesimal isometries* of a given manifold M . In our context, we focus on M being either the plane \mathbb{R}^2 or the two-sphere S^2 , defining our domain for 2D unsteady flow fields. Corresponding to the notion of physically-realizable observers, we can therefore describe all possible observer motions by (time-dependent) Killing vector fields. Every motion described by a

• Xingdi Zhang, Markus Hadwiger, and Peter Rautek are with King Abdullah University of Science and Technology (KAUST), Visual Computing Center, Thuwal, 23955-6900, Saudi Arabia. E-mail: { xingdi.zhang, markus.hadwiger, peter.rautek } @kaust.edu.sa.
• Thomas Theußl is with King Abdullah University of Science and Technology (KAUST), Core Labs, Thuwal, 23955-6900, Saudi Arabia. E-mail: thomas.theussl@kaust.edu.sa.

Manuscript received 31 Mar. 2021; accepted xx xxx. 201x. Date of Publication xx xxx. 201x; date of current version xx xxx. 201x. For information on obtaining reprints of this article, please send e-mail to: reprints@ieee.org. Digital Object Identifier: xx.xxxx/TVCG.201x.xxxxxxx

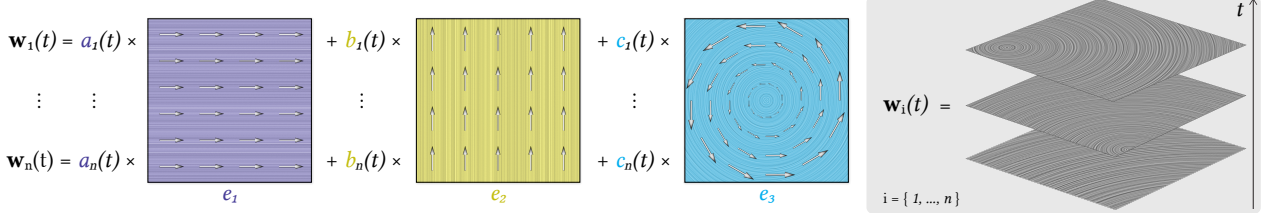


Fig. 2. Observer representation. Any physically-realizable observer is determined by a time-dependent Killing field $(x, t) \mapsto \mathbf{w}(x, t) = a(t)\mathbf{e}_1(x) + b(t)\mathbf{e}_2(x) + c(t)\mathbf{e}_3(x)$. The basis vector fields \mathbf{e}_1 (purple), \mathbf{e}_2 (yellow), and \mathbf{e}_3 (cyan) are steady vector fields that do not change over time. Any possible (time-dependent) observer \mathbf{w}_i is solely determined by a time-dependent function $t \mapsto (a_i(t), b_i(t), c_i(t))$ of three scalar coefficients (a_i, b_i, c_i) per time t .

Killing field is guaranteed to be physically realizable. Any observer that cannot be modeled by a Killing field is not physically realizable.

Lie algebra of observer motions. A Lie algebra [12] is a vector space, of abstract vector objects with scalar multiplication and vector addition, plus an additional vector product, the Lie bracket $[\cdot, \cdot]$. In our context, however, each vector (element) of a Lie algebra represents an entire vector *field* on the underlying manifold M . This enables us to represent all physically-realizable observer motions as elements of the Lie algebra of Killing fields on the manifold M . Most importantly, as a vector space, every Lie algebra has a basis. Therefore, any observer motion can be given as a linear combination of *basis Killing fields*.

Notation. We denote vectors and vector fields in bold, like \mathbf{v} , \mathbf{u} , and real numbers as well as spatial points in non-bold, like a , t , or $x \in M$.

Our framework

For both the manifolds $M = \mathbb{R}^2$ and $M = \mathbb{S}^2$, respectively, the Lie algebra of physically-realizable observer motions is three-dimensional (as a vector space). Thus, all possible observer motions are fully determined by coefficients referred to a three-dimensional basis. We choose a fixed basis of three *basis Killing vector fields* $\{\mathbf{e}_1, \mathbf{e}_2, \mathbf{e}_3\}$ on M , and represent every possible observer motion by three real coefficients (a, b, c) for each time t . Any observer is therefore determined by a function

$$t \mapsto (a(t), b(t), c(t)). \quad (1)$$

The corresponding observer motion is given by a time-dependent Killing vector field \mathbf{w} , determining the motion via its derivative, as

$$(x, t) \mapsto \mathbf{w}(x, t) = a(t)\mathbf{e}_1(x) + b(t)\mathbf{e}_2(x) + c(t)\mathbf{e}_3(x). \quad (2)$$

See Fig. 2. This representation enables averaging, interpolating, and comparing observers simply via their coefficients given by Eq. 1.

1.2 Interactive Exploration Pipeline

Fig. 3 depicts an overview of our interactive exploration framework. The goal is to explore an arbitrary, unsteady input flow field \mathbf{v} . However, in order to do so, we want to be able to use an arbitrary reference frame, relative to which the field \mathbf{v} is visualized, and features such as vortices can be computed objectively. To facilitate this, the second input to our system is another unsteady flow field \mathbf{u} , which is used with the semantics of an *observer field* [18]. We can initialize the field \mathbf{u} by computing (or loading) the solution of an objective optimization [14, 18, 39], but we can also simply use the field $\mathbf{u} := \mathbf{v}$. The latter can be used to “extract” observers from the input field \mathbf{v} itself. Independent of how the observer field \mathbf{u} is initialized, our framework represents all observers \mathbf{w} by functions $t \mapsto (a(t), b(t), c(t))$ (Eq. 1), determining observers by either (1) extraction from the observer field \mathbf{u} ; or (2) averaging or interpolation of already known observers. When an observer is chosen interactively, the input field \mathbf{v} can immediately be visualized relative to it. Furthermore, we can visualize the functions $t \mapsto (a(t), b(t), c(t))$ as curves in the three-dimensional parameter space $(a, b, c) \subset \mathbb{R}^3$ (Fig. 3 (center)).

1.3 Observers and Objectivity

A fundamental property of our framework is that we determine observers objectively, in the sense that all possible observers agree on which specific reference frame motions were chosen¹. This has the consequence that properties of the input field computed relative to any one

¹We call these *objectively-determined observers*. This is not a standard term, but it captures the concept well. Appendix B provides a detailed discussion.

such observer are objective. Furthermore, because all our observers are physically realizable, these properties are therefore also physically observable. Our observers are determined objectively because we “extract” them along path lines of the observer field \mathbf{u} , which are Lagrangian and thus objective [21], and because of a crucial theorem about Killing fields (Theorem 3.2). However, this only holds when all possible observers do, in fact, agree on the motion described by the field \mathbf{u} . This is trivially the case when we choose $\mathbf{u} := \mathbf{v}$. Crucially, however, the same is true when \mathbf{u} is computed via objective optimization, as those of Günther et al. [14], Hadwiger et al. [18], or Rautek et al. [39]. Furthermore, we allow determining new observers by averaging or interpolation of a set of observers. If the latter are all objectively determined, the resulting new observer is again objectively determined. For more details and some subtleties, we refer to Appendix B (supplementary material).

1.4 Contributions

We propose the first framework for the interactive, objective exploration of unsteady 2D flow from the perspective of a set of physically-realizable observers. In contrast to prior work that uses a large number of observers jointly, such as one observer per space-time grid point [14], or a continuous field of observers [18, 39], we focus on facilitating visualization and feature detection with respect to individual observers.

In particular, we for the first time (1) enable the interactive selection, comparison, and user evaluation of objective vortex structures relative to an interactively-chosen and modified set of physically-realizable observers; (2) define a novel mathematical framework that enables the efficient manipulation of observers by expressing all possible observer motions in the same basis of vector fields for the corresponding Lie algebra; (3) describe how previous methods integrate with our interactive framework; and (4) leverage the Lie algebra of observer motions to treat flow fields in 2D flat space and the curved surface of a sphere, e.g., for geophysical flow fields, respectively, in a conceptually unified way.

2 RELATED WORK

Flow visualization is one of the core topics of scientific visualization, and many techniques have been developed over the years to visualize flow fields, for example LIC for steady (time-independent) flow fields [8], or texture advection methods for unsteady (time-dependent) flow fields [25, 47], as well as the visualization of integral curves [26, 49]. Instead of flow visualization in general, in this section we focus on related work whose specific aspects are most relevant to our work.

Reference frames. Flow fields are velocity vector fields, and therefore they can only be given with respect to a frame of reference, or an observer. One important area where this fact is important is in the detection and visualization of vortices, where it has become a major consideration when evaluating different vortex detection methods [17, 19]. A crucial notion is that of the invariance of a given method with respect to a particular kind of reference frame transformation, for example Galilean invariance [48], rotation invariance [15], or invariance relative to rigid motions [19]. The latter is known as *objectivity* [19] or *frame indifference* [46], originally defined in continuum mechanics [22, 33, 46], and recognized to be of fundamental importance for vortex detection more recently [14, 17, 19, 21], although used earlier as well [1, 11].

Multiple reference frames. Most commonly, only a single reference frame is considered for flow visualization or computational tasks such as vortex detection. Several recent methods, however, jointly consider multiple reference frames, such as averaging observers related to a

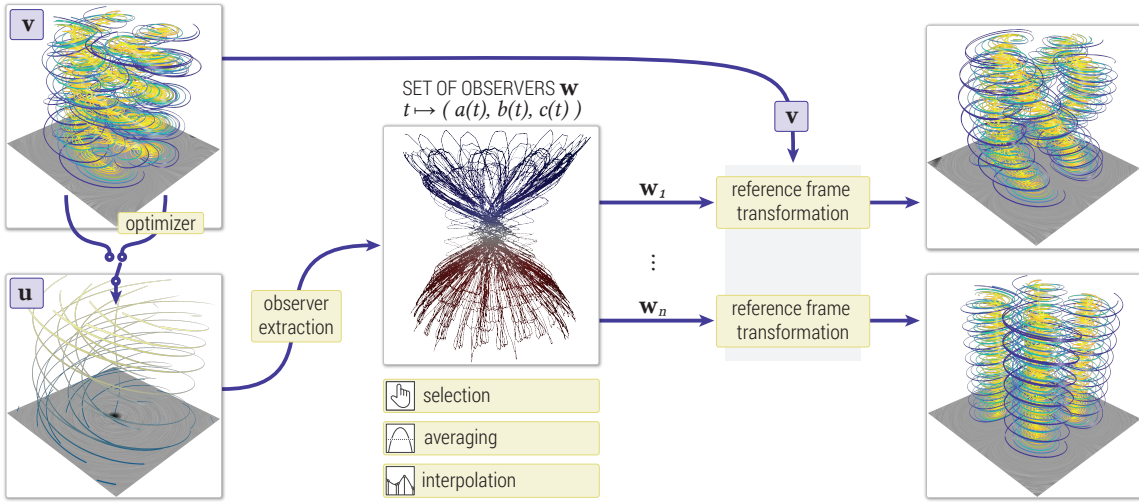


Fig. 3. Interactive exploration pipeline. The input to our system consists of two unsteady vector fields: the input flow field \mathbf{v} , and an *observer field* \mathbf{u} . The observer field can be computed via objective optimization [14, 18], or can be initialized to $\mathbf{u} := \mathbf{v}$ (to extract observers from the input field). Observers are extracted from the field \mathbf{u} , representing each corresponding Killing field \mathbf{w} by a function $t \mapsto (a(t), b(t), c(t))$. New observers can be generated by averaging or interpolation. When an observer is selected, the input field \mathbf{v} can be visualized interactively *relative* to that observer.

finite set of Galilean-invariant critical points [7], one observer per point in space-time [14], or a continuous field of observers [18, 39].

Vortex detection. Vortices are important features in flow visualization [17] and fluid mechanics [41]. There is no single, well-defined notion of a vortex, but they are usually seen as a swirling motion around a central region [1, 10, 29, 40]. Earlier methods have often used only spatial (in contrast to time) derivatives, e.g., the well-known methods of Okubo [34] and Weiss [50], Sujudi and Haimes [44], the Q Criterion of Hunt et al. [23], or the λ_2 criterion of Jeong and Hussain [24], which can lead to challenges for unsteady flow. One reason for this is that many early methods are partially based on critical point theory of steady vector fields [36, 37]. Later extensions were improved for unsteady flow, e.g., with Galilean invariance [42, 48], often building on the parallel vectors operator [35] or a predictor-corrector approach [5]. Criteria can be grouped into *line-based* vs. *region-based* techniques [17], the latter often including the detection of region boundaries [13, 21]. The objectivity of vortex criteria is now seen to be a crucial desired property of vortex detectors [14, 17, 19, 21]. One particular recent example that we also use is the Lagrangian-Averaged Vorticity Deviation (LAVD) [21].

Generic objectivization. A recent idea for developing vortex detection methods that are objective is to solve an optimization problem that enables *generically “objectivizing”* non-objective vortex criteria [4, 14, 16, 18, 39]. All of these approaches perform objective computations that define a large number of observers. The motivation for this is the well-established understanding that for many flow fields a single observer is not able to depict all vortices of interest [29]. However, while the objectivity of these approaches guarantees that any physically-realizable, i.e., rigidly-moving, observer will reach the same conclusions regarding the “joint” detection of vortices, none of these methods guarantees that there is *one physically-realizable observer* that by itself (i.e., not jointly) would have computed the same vortex using physically-motivated criteria. While this does not change the fact that the above methods are provably objective [14, 18, 39, 45], recent work has argued that physical criteria should also be used to determine the validity and consistency of vortex detection [20]. In this work, we approach this problem from a different perspective to try and combine the advantages of both viewpoints: We enable the interactive exploration of multiple, objectively-determined observers, but allow users to choose specific, physically-realizable observers for actual vortex detection and visualization. In this way, physically-motivated criteria fully apply.

Killing vector fields. The properties of Killing fields are often explored in Riemannian geometry [9, 32, 38]. They have been used explicitly in geometry [6, 28, 31, 43], including vector field design on curved surfaces [2, 3], and recently also in flow visualization [18, 39].

3 OBSERVERS AND SETS OF OBSERVERS

Our approach is based on a set of *physically-realizable* observers. In this section, we describe how these observers are modeled as Killing vector fields, and how the corresponding description can be extracted from any given input observer velocity field \mathbf{u} (Fig. 3, bottom left).

3.1 Physically-Realizable Observers

The central basic notion of this paper is given by the following

Theorem 3.1. *An observer is physically realizable if its time-dependent motion relative to any other physically-realizable observer is a rigid motion, i.e., if the map between the two reference frames is an isometry.*

This basically means that every rigid reference frame motion corresponds to a physically-realizable observer. The reason for the “circular” argument above is that all motion is relative, and thus for a rigid motion to in fact describe a physical observer, the background reference frame (e.g., the lab frame) must already be known to be physically realizable. In terms of our input field \mathbf{v} , this means that the whole field must have been measured relative to the same, physically-realizable observer.

Killing vector fields

A vector field $x \mapsto \mathbf{w}(x)$ is a Killing field, if its (spatial) velocity gradient $\nabla \mathbf{w}$ is identically *anti-symmetric*. That is, when for \mathbf{w} we have

$$\langle \nabla \mathbf{w}(\mathbf{x}), \mathbf{x} \rangle = 0. \quad (3)$$

This must hold at all points $x \in M$, for all vectors \mathbf{x} . Eq. 3 is valid for all manifolds M , with $\nabla \mathbf{w}$ the *covariant derivative* of \mathbf{w} (in components, $\nabla_j w^i$; see Rautek et al. [39] for details). For $M = \mathbb{R}^2$ with Cartesian coordinates, $\nabla \mathbf{w}$ is simply a Jacobian matrix $\partial_j w^i$ of partial derivatives.

Time-dependent Killing fields

We define a *time-dependent* Killing field with the properties given above to hold for each fixed time t , giving a time-dependent field

$$(x, t) \mapsto \mathbf{w}(x, t). \quad (4)$$

Corollary 3.1. *A time-dependent Killing field $\mathbf{w}(x, t)$ gives the derivative of a time-dependent rigid motion. Therefore, it corresponds to a physically-realizable observer, defined by integrating the Killing field.*

As above, it is important that \mathbf{w} is measured relative to a physically-realizable observer. We will also exploit the following important

Theorem 3.2. *A Killing field \mathbf{w} is uniquely defined by: (1) a single vector $\mathbf{w}(x)$ at an arbitrarily chosen point $x \in M$, and (2) the corresponding (anti-symmetric) velocity gradient $(\nabla \mathbf{w})_x$ at the same point x .*

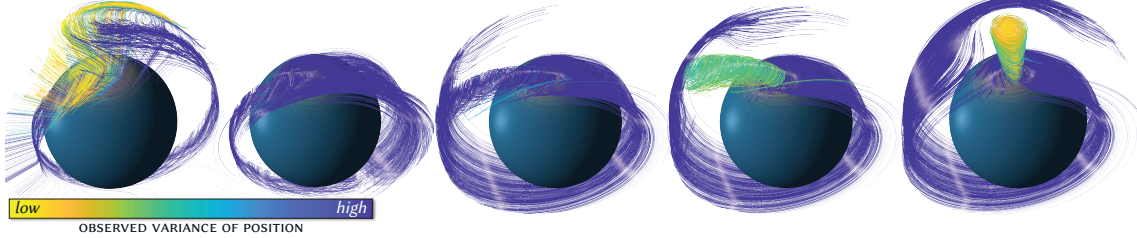


Fig. 4. Vortex on the sphere. We exploit the same 3D vector space structure of the Lie algebra of observer motions on spherical domains as in the plane. Here, we smoothly interpolate between two observers, the input lab frame (left) and an objectively-determined observer [39] (right), smoothly “shifting” the observed field and the contained vortex until the latter becomes visible (right). (The axis orthogonal to the sphere corresponds to time.)

This is a well-known property of Killing fields [38, p.315]. However, this property is crucial to objectively “extracting” physically-realizable observers from the methods described in prior work [14, 18, 39], and converting them to the representation of our framework. See Sec. 3.3.

3.2 The Lie Algebra of Observer Motions

We exploit that the Lie algebras of Killing fields on our manifolds M of interest, the plane \mathbb{R}^2 and the sphere \mathbb{S}^2 , are three-dimensional vector spaces, and thus have 3D vector space bases. (See also Appendix A.)

Dimensionality and basis expansion

It is crucial to note that the Lie algebra of Killing fields is a vector space of vector fields, i.e., each element (abstract vector) of this vector space is itself a whole *vector field* on the underlying manifold M . It is also in this sense that the Lie algebras that we use are three-dimensional: Each Killing field can be referred to a basis comprising three *basis vector fields*, each weighted by a scalar coefficient. We have the following

Theorem 3.3. *A Killing field w on a manifold M is uniquely defined by a spanning set of basis Killing fields $\{\mathbf{e}_i\}$ and the corresponding set of coefficients $\{w^i\}$. The Killing field w is then given as $w = \sum_i w^i \mathbf{e}_i$.*

In this paper, all vector spaces of Killing fields are three-dimensional, and we will therefore only need three coefficients w^i , which we will instead denote by $a := w^1, b := w^2, c := w^3$, or collectively by (a, b, c) .

Inner products of vector fields

To be able to determine orthogonality of basis functions as well as for comparing observers by comparing their corresponding Killing fields, we will make use of an inner product between vector fields, defined on the Lie algebra of observer motions. We define the inner product between two (Killing) vector fields \mathbf{w}_1 and \mathbf{w}_2 , with domain D , by

$$\langle\langle \mathbf{w}_1, \mathbf{w}_2 \rangle\rangle := \int_D \langle \mathbf{w}_1, \mathbf{w}_2 \rangle_x dA. \quad (5)$$

Here, the usual inner product in the tangent space at each point $x \in D$ is denoted by $\langle \cdot, \cdot \rangle_x$, and dA denotes integration over area elements. This inner product is defined with respect to a domain $D \subseteq M$. For $M = \mathbb{S}^2$, we use $D = \mathbb{S}^2$, because \mathbb{S}^2 is compact and the integral is therefore guaranteed to be finite. For $M = \mathbb{R}^2$, we typically integrate over a compact rectangular subdomain $D = [x_a, x_b] \times [y_a, y_b] \subset \mathbb{R}^2$.

Efficient computation of inner products

Instead of computing the above integrals for every arbitrary pair of observers $(\mathbf{w}_1, \mathbf{w}_2)$, we can exploit the vector space structure of the Lie algebra of Killing fields. From this structure, we know that every Killing field can be written as a linear combination $\mathbf{w} = \sum_i w^i \mathbf{e}_i$, where the \mathbf{e}_i are basis Killing vector fields on the manifold M . Using the inner product $\langle\langle \cdot, \cdot \rangle\rangle$ between two vector fields given by Eq. 5, we can define a metric tensor g_{ij} of Killing vector fields, given by the components

$$g_{ij} := \langle\langle \mathbf{e}_i, \mathbf{e}_j \rangle\rangle. \quad (6)$$

Given this metric tensor, we can then compute the inner product between any two Killing fields simply from their components as

$$\langle\langle \mathbf{w}_1, \mathbf{w}_2 \rangle\rangle = \sum_{i,j} g_{ij} w_1^i w_2^j. \quad (7)$$

For more details, we refer to Appendix C (supplementary material).

Basis Killing fields in the Euclidean plane

The Lie algebra of Killing fields on $M = \mathbb{R}^2$ is three-dimensional, and we construct the following three linearly-independent basis Killing fields in \mathbb{R}^2 , where the vectors at any point $x = (\hat{x}, \hat{y}) \in \mathbb{R}^2$ are

$$\mathbf{e}_1(\hat{x}, \hat{y}) = \begin{bmatrix} 1 \\ 0 \end{bmatrix}, \quad \mathbf{e}_2(\hat{x}, \hat{y}) = \begin{bmatrix} 0 \\ 1 \end{bmatrix}, \quad \mathbf{e}_3(\hat{x}, \hat{y}) = \begin{bmatrix} 0 & -1 \\ 1 & 0 \end{bmatrix} \begin{bmatrix} \hat{x} \\ \hat{y} \end{bmatrix}. \quad (8)$$

See Fig. 2. For the field \mathbf{e}_3 , corresponding to v being given on a rectangular domain $D = [x_a, x_b] \times [y_a, y_b] \subset \mathbb{R}^2$, with center point $(\hat{x}_0, \hat{y}_0) = \frac{1}{2}(x_a + x_b, y_a + y_b)$, we have defined $(\bar{x}, \bar{y}) := (\hat{x} - \hat{x}_0, \hat{y} - \hat{y}_0)$.

Each basis element must be a Killing field. To confirm, we compute

$$\nabla \mathbf{e}_1 = 0, \quad \nabla \mathbf{e}_2 = 0, \quad \nabla \mathbf{e}_3 = \begin{bmatrix} 0 & -1 \\ 1 & 0 \end{bmatrix}. \quad (9)$$

Therefore, Eq. 3 indeed holds for all fields \mathbf{e}_i , i.e., we have

$$\langle\langle \nabla \mathbf{e}_i(\mathbf{x}), \mathbf{x} \rangle\rangle = 0, \quad (10)$$

for all $i \in \{1, 2, 3\}$, and for all vectors \mathbf{x} , at all points $x \in M = \mathbb{R}^2$.

Using this basis, we can therefore write any Killing field \mathbf{w} on $M = \mathbb{R}^2$ as $\mathbf{w} = a\mathbf{e}_1 + b\mathbf{e}_2 + c\mathbf{e}_3$, with three coefficients (a, b, c) . We note that, due to this particular choice of basis, (a, b) have the meaning of a linear velocity vector (given with two Cartesian components), and the third coefficient c has the meaning of angular velocity.² In fact, the linear velocity is the same constant vector at all points $x \in \mathbb{R}^2$.

Orthogonality. Due to symmetry, this basis is orthogonal for a rectangular domain of integration with (\hat{x}_0, \hat{y}_0) chosen in the center, where, in particular, we have $\langle\langle \mathbf{e}_1, \mathbf{e}_3 \rangle\rangle = \langle\langle \mathbf{e}_2, \mathbf{e}_3 \rangle\rangle = 0$, because $\langle \mathbf{e}_1(\bar{x}, \bar{y}), \mathbf{e}_3(\bar{x}, \bar{y}) \rangle = -\langle \mathbf{e}_1(-\bar{x}, -\bar{y}), \mathbf{e}_3(-\bar{x}, -\bar{y}) \rangle$, and likewise for the fields \mathbf{e}_2 and \mathbf{e}_3 . The orthogonality $\langle\langle \mathbf{e}_1, \mathbf{e}_2 \rangle\rangle = 0$ immediately follows from the orthogonality $\langle \mathbf{e}_1(\hat{x}, \hat{y}), \mathbf{e}_2(\hat{x}, \hat{y}) \rangle = 0$ at every point (\hat{x}, \hat{y}) .

See Eq. 5 for the definition of the vector field inner product $\langle\langle \cdot, \cdot \rangle\rangle$.

Basis Killing fields on the sphere

The Lie algebra of Killing fields on $M = \mathbb{S}^2$ is also three-dimensional. We construct the following three basis Killing fields for the two-sphere $\mathbb{S}^2 := \{(\hat{x}, \hat{y}, \hat{z}) | \hat{x}^2 + \hat{y}^2 + \hat{z}^2 = 1\}$ embedded in \mathbb{R}^3 , where the vectors at any point $x = (\hat{x}, \hat{y}, \hat{z})$, as elements of the tangent space embedded in \mathbb{R}^3 at that point, are given by (see Fig. 10 in the supplementary material)

$$\begin{aligned} \mathbf{e}_1(\hat{x}, \hat{y}, \hat{z}) &= \begin{bmatrix} 0 & 0 & 0 \\ 0 & 0 & -1 \\ 0 & 1 & 0 \end{bmatrix} \begin{bmatrix} \hat{x} \\ \hat{y} \\ \hat{z} \end{bmatrix}, \quad \mathbf{e}_3(\hat{x}, \hat{y}, \hat{z}) = \begin{bmatrix} 0 & -1 & 0 \\ 1 & 0 & 0 \\ 0 & 0 & 0 \end{bmatrix} \begin{bmatrix} \hat{x} \\ \hat{y} \\ \hat{z} \end{bmatrix}, \\ \mathbf{e}_2(\hat{x}, \hat{y}, \hat{z}) &= \begin{bmatrix} 0 & 0 & 1 \\ 0 & 0 & 0 \\ -1 & 0 & 0 \end{bmatrix} \begin{bmatrix} \hat{x} \\ \hat{y} \\ \hat{z} \end{bmatrix}. \end{aligned} \quad (11)$$

Using this basis, we can write any Killing field \mathbf{w} on $M = \mathbb{S}^2$ as $\mathbf{w} = a\mathbf{e}_1 + b\mathbf{e}_2 + c\mathbf{e}_3$, with three coefficients (a, b, c) . We note that, due to the above choice of basis, the coefficients (a, b, c) determine a 3D angular velocity vector, and $\omega^2 := a^2 + b^2 + c^2$ is the corresponding

²As for any vector space, other bases are of course also possible. Here then, however, no single coefficient would be the angular velocity. See Appendix A.

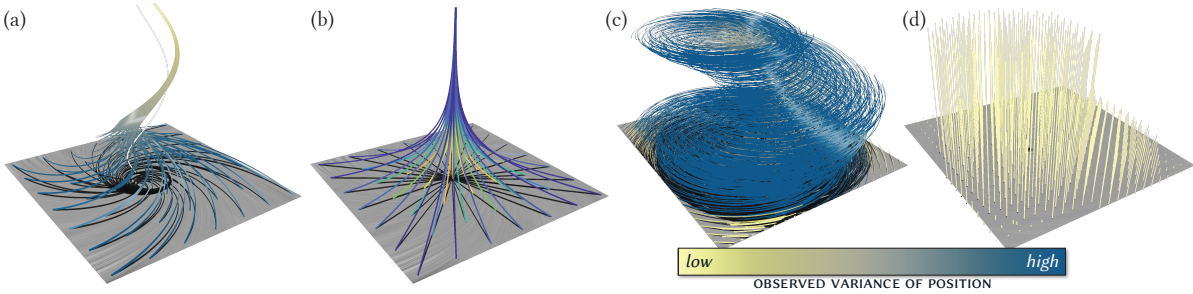


Fig. 5. Beads flow. (Original; a, b) The input flow field (vertical axis is time) contains rotational as well as contracting motion (negative divergence). However, using our framework one can determine that all rotational parts of this field can be fully explained by a rotating reference frame. (Divergence-free; c, d) Observer exploration enables us to see that, in fact, this flow field is itself a Killing field. Thus, the input field (c) can be explained purely by a moving reference frame observing a 0-field (d). This indicates that this field does not contain any intrinsic motion, beyond the motion of an observer.

(squared) angular velocity (magnitude). Since Eq. 3 is intrinsically defined in each tangent space, to see that the 2D tensors $\nabla \mathbf{e}_i$ are anti-symmetric, we must compute the covariant derivatives $\nabla \mathbf{e}_i$ at all $x \in \mathbb{S}^2$. Using a right-handed orthonormal basis in each tangent plane, they are

$$(\nabla \mathbf{e}_i)_x = \begin{bmatrix} 0 & -\cos \varphi_i(x) \\ \cos \varphi_i(x) & 0 \end{bmatrix}. \quad (12)$$

Here, the angle $\varphi_i(x) \in [0, \pi]$ is the colatitude of x away from the “north pole” of the respective \mathbf{e}_i , i.e., $\hat{x} = 1$ for \mathbf{e}_1 , $\hat{y} = 1$ for \mathbf{e}_2 , $\hat{z} = 1$ for \mathbf{e}_3 . Therefore, Eq. 3 again holds for all \mathbf{e}_i , i.e., $\langle \nabla \mathbf{e}_i(\mathbf{x}), \mathbf{x} \rangle = 0$ for all \mathbf{x} .

Orthogonality. This basis is also orthogonal, i.e., $\langle \langle \mathbf{e}_i, \mathbf{e}_j \rangle \rangle = 0$ for all $i \neq j$. This can be confirmed by analytic integration over the sphere.

Representation of observers

We define an observer as the time-dependent, rigid reference frame motion given by a time-dependent Killing field \mathbf{w} . Instead of storing an explicit vector field $(x, t) \mapsto \mathbf{w}(x, t)$ for each observer, we store observers with respect to a chosen basis of Killing fields. While in principle this basis is arbitrary, we use the basis vector fields given by Eq. 8 (for Euclidean domains $M = \mathbb{R}^2$), and Eq. 11 (for spherical domains $M = \mathbb{S}^2$), respectively. Any given observer \mathbf{w} is thus given by a function $t \mapsto ((a(t), b(t), c(t)))$ (Eq. 1), which at any time allows us to obtain the corresponding time-dependent Killing field \mathbf{w} from Eq. 2.

Comparing observers

We exploit the low-dimensional (in our case, three-dimensional) vector space structure of Killing vector fields in order to efficiently quantify the similarity of two observers given as time-dependent Killing fields.

First, from the definition of the inner product of two vector fields given by Eq. 5, we can define the difference between two arbitrary (time-independent) Killing fields as the scalar-valued distance function

$$d(\mathbf{w}_1, \mathbf{w}_2) := \sqrt{\langle \langle \mathbf{w}_1 - \mathbf{w}_2, \mathbf{w}_1 - \mathbf{w}_2 \rangle \rangle}. \quad (13)$$

This definition in fact defines a *metric* on the vector space of all Killing fields in the domain $D \subseteq M$, where we want to compare observers. For time-dependent Killing fields $\mathbf{w}_1(x, t)$ and $\mathbf{w}_2(x, t)$, we now define

$$d(\mathbf{w}_1(t), \mathbf{w}_2(t); t_0, t_1) := \int_{t_0}^{t_1} d(\mathbf{w}_1(t), \mathbf{w}_2(t)) dt. \quad (14)$$

Here, we have integrated over a desired time window $[t_0, t_1]$, over which we want to compare the two observers. The rationale for this definition is simply that we integrate the per-time distance values over a time window of interest, in order to quantify the “total” difference between the two observers over that time window. (Longer time windows, in general, give larger distances, when the two fields are different.)

We note that when both \mathbf{w}_1 and \mathbf{w}_2 are objectively-determined observers, then both distance functions above give *objective* scalars.

3.3 Determination of Observer Sets

We can store a set of observers by storing multiple observers, each represented by a function $t \mapsto (a(t), b(t), c(t))$, as above (Eq. 1).

However, we can also “extract” an arbitrary number of observers from a given vector field, which we will refer to as the *observer field* \mathbf{u} .

Observer world lines

Theorem 3.2 shows that an observer can also be specified by a function

$$t \mapsto (x(t), \mathbf{w}(x(t), t), (\nabla \mathbf{w})_{(x(t), t)}), \quad (15)$$

where $t \mapsto x(t)$ is an arbitrary path on the manifold M , and we prescribe the corresponding vectors \mathbf{w} , and tensors $\nabla \mathbf{w}$ along this path. Although compared to Eq. 1, the above representation requires more storage, this way of specifying Killing fields enables the following general approach for extracting observers from a given observer velocity field \mathbf{u} .

Observer world lines from observer fields

It is possible to avoid storing the path $t \mapsto x(t)$ in the previous definition by defining it as the path line of a vector field $\mathbf{u}(x(t), t)$ given along the path $x(t)$, which is obtained by solving the non-autonomous ODE

$$\frac{d}{dt} x(t) = \mathbf{u}(x(t), t), \quad (16)$$

with an initial value $x(t_0)$, i.e., some chosen position on the path line $t \mapsto x(t)$ at time $t = t_0$, for some chosen time t_0 . We call this path $t \mapsto x(t)$ a *world line* [18] of the corresponding observer. In order to extract an observer, at each time t we refer to the corresponding point $x(t)$.

Extraction from observer field in the Euclidean plane

Given a single vector $\mathbf{u}(x)$ and the velocity gradient $(\nabla \mathbf{u})_x$ at any point $x \in M = \mathbb{R}^2$, we can extract the coefficients of the corresponding Killing field \mathbf{w} , with respect to the basis fields $\{\mathbf{e}_1, \mathbf{e}_2, \mathbf{e}_3\}$ (Eq. 8), as

$$\nabla \mathbf{w} = \frac{1}{2} \left((\nabla \mathbf{u})_x - (\nabla \mathbf{u})_x^T \right) = \begin{bmatrix} 0 & -c \\ c & 0 \end{bmatrix}, \quad \mathbf{u}(x) + \nabla \mathbf{w}(\mathbf{r}) = \begin{bmatrix} a \\ b \end{bmatrix}. \quad (17)$$

We define $\mathbf{r} := (\hat{x}_0 - \hat{x}, \hat{y}_0 - \hat{y})^T$, with (\hat{x}, \hat{y}) the Cartesian coordinates of the point x , and (\hat{x}_0, \hat{y}_0) the center point used in the definition of the basis vector field \mathbf{e}_3 . The coefficients (a, b, c) now determine the Killing field $\mathbf{w} = a\mathbf{e}_1 + b\mathbf{e}_2 + c\mathbf{e}_3$, referred to the basis given in Eq. 8.

Extraction from observer field on the sphere

Given a single vector $\mathbf{u}(x)$ and the covariant derivative $(\nabla \mathbf{u})_x$ at any point $x \in M = \mathbb{S}^2$, we can extract the coefficients of the corresponding Killing field \mathbf{w} , with respect to the basis fields $\{\mathbf{e}_1, \mathbf{e}_2, \mathbf{e}_3\}$ (Eq. 11), using the following approach. Referring to the point $x \in \mathbb{S}^2$ as the position vector $\mathbf{r}(x) := (\hat{x}, \hat{y}, \hat{z})^T$ in Cartesian coordinates, we can define the following orthonormal basis, written as column vectors of the matrix

$$\hat{\mathbf{B}} := [\mathbf{x} \mid \mathbf{z} \times \mathbf{x} \mid \mathbf{z}], \quad \mathbf{x} := \mathbf{u}(x)/\|\mathbf{u}(x)\|, \quad \mathbf{z} := \mathbf{r}(x). \quad (18)$$

When $\|\mathbf{u}(x)\| = 0$, \mathbf{x} can be any unit vector in the tangent plane at x . Given the covariant derivative $\nabla \mathbf{u}$ in components as $\nabla_j u^i$ in some coordinate chart with tangent space basis $\{\mathbf{b}_1, \mathbf{b}_2\}$ at x , and the coordinate

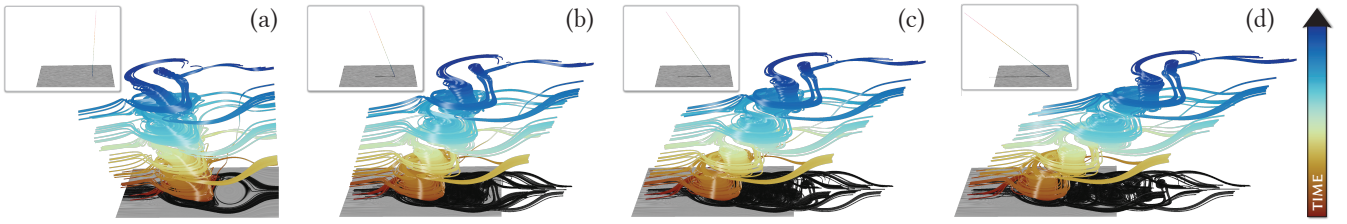


Fig. 6. Cylinder flow. The vortex structures in this data set are short-lived. They appear and disappear frequently over time. In the input lab frame (a) different vortices overlap (over time) around the same spatial position and appear to be the same vortex. We interpolate (a-d) between the lab frame and an objectively-determined constant-velocity observer that “comoves” with the vortices, revealing them more clearly. The insets depict observer world lines. Time corresponds to the vertical axis and is also color-coded to help highlight how individual vortices appear and disappear over time.

Jacobian \mathbf{J} transforming from that basis to the basis $\hat{\mathbf{B}}$, we can compute³

$$\nabla_j \hat{u}^i = \mathbf{J} (\nabla_j u^i) \mathbf{J}^{-1}, \quad \nabla_j \hat{w}^i = \frac{1}{2} (\nabla_j \hat{u}^i - \nabla_i \hat{u}^j) = \begin{bmatrix} 0 & -\hat{c} \\ \hat{c} & 0 \end{bmatrix}. \quad (19)$$

Given the chart tangent space basis $\{\mathbf{b}_1, \mathbf{b}_2\}$, embedded in \mathbb{R}^3 , the Jacobian \mathbf{J} is given by the top-left 2×2 submatrix of the 3×3 matrix

$$\hat{\mathbf{J}} = \hat{\mathbf{B}}^T [\mathbf{b}_1 \mid \mathbf{b}_2 \mid \mathbf{z}]. \quad (20)$$

From the obtained \hat{c} , and the length $\hat{b} := \|\mathbf{u}(x)\|$, we can now compute

$$\hat{\mathbf{K}} = \begin{bmatrix} 0 & -\hat{c} & \hat{b} \\ \hat{c} & 0 & 0 \\ -\hat{b} & 0 & 0 \end{bmatrix}, \quad \mathbf{K} = \hat{\mathbf{B}} \hat{\mathbf{K}} \hat{\mathbf{B}}^T = \begin{bmatrix} 0 & -c & b \\ c & 0 & -a \\ -b & a & 0 \end{bmatrix}. \quad (21)$$

The coefficients (a, b, c) obtained from the matrix \mathbf{K} now determine the Killing field $\mathbf{w} = a\mathbf{e}_1 + b\mathbf{e}_2 + c\mathbf{e}_3$, referred to the basis given in Eq. 11.

For completeness, we note that here $\hat{b} = \omega \sin \varphi$ and $\hat{c} = \omega \cos \varphi$, where $\omega^2 = \hat{b}^2 + \hat{c}^2 = a^2 + b^2 + c^2$ is the (squared) angular velocity of the global rotation of the sphere given by \mathbf{w} , with φ the colatitude of x relative to the critical point of \mathbf{w} that is the “north pole” of the rotation, i.e., the point $(\bar{x}, \bar{y}, \bar{z})^T = (a, b, c)^T / \|(a, b, c)^T\|$, defined when $\omega \neq 0$.

4 OBSERVER AVERAGING AND INTERPOLATION

Using the vector space structure of all observer Killing fields, we can directly average a set of observers and interpolate between observers.

4.1 Observer Averaging

Given a set of observers $\{\mathbf{w}_i\}_{i \in I}$ with the index $i \in I$ from some index set I , considering the vector space structure of the space of all observers, we can simply define the *average observer* of this set of observers as

$$t \mapsto (\bar{a}(t), \bar{b}(t), \bar{c}(t)) := \frac{1}{|I|} \left(\sum_{i \in I} a_i(t), \sum_{i \in I} b_i(t), \sum_{i \in I} c_i(t) \right), \quad (22)$$

where $|I|$ is the cardinality of the index set I . If I is a whole region of a manifold M instead of a discrete set, we define the above average with integrals instead of sums, and the cardinality for normalization by an appropriate *measure* of the set I , e.g., the area measure on M .

Sec. 6.3 describes an application of this averaging technique, applied over a region $I = U(t) \subset \mathbb{R}^2$, with the standard area measure on \mathbb{R}^2 .

4.2 Direct Observer Interpolation (Blending)

Given two observers $\mathbf{w}_1 = a_1 \mathbf{e}_1 + b_1 \mathbf{e}_2 + c_1 \mathbf{e}_3$ and $\mathbf{w}_2 = a_2 \mathbf{e}_1 + b_2 \mathbf{e}_2 + c_2 \mathbf{e}_3$, we can directly interpolate between them via ($\alpha \in [0, 1]$)

$$\begin{aligned} \mathbf{w}(t; \alpha) = & ((1 - \alpha)a_1(t) + \alpha a_2(t)) \mathbf{e}_1 + \\ & ((1 - \alpha)b_1(t) + \alpha b_2(t)) \mathbf{e}_2 + \\ & ((1 - \alpha)c_1(t) + \alpha c_2(t)) \mathbf{e}_3. \end{aligned} \quad (23)$$

³We note that the anti-symmetrization used here depends on the fact that the basis $\hat{\mathbf{B}}$ is orthonormal, and hence the corresponding metric tensor is the identity. Otherwise, $\nabla_j u_i$ and the metric g_{ij} would have to be used explicitly. See [39].

Due to the linearity of the Lie algebra of Killing fields, this works for both $M = \mathbb{R}^2$ and $M = \mathbb{S}^2$, by using the corresponding basis $\{\mathbf{e}_i\}$.

See Fig. 6 for an example, where we directly interpolate between the (input) lab frame observer (given by the observer field $\mathbf{u} = 0$) and an observer “comoving” along with the vortices. (However, see Appendix B for additional discussion on using the lab frame observer.)

4.3 Observer Interpolation Along a Path

Given an arbitrary observer field \mathbf{u} , we can pick two points $x_1(t) \in M$ and $x_2(t) \in M$, respectively, for an arbitrarily chosen fixed time t . We can then extract observers corresponding to any interpolated point $x(t; \alpha) \in M$, in between the two points. For simplicity, for $M = \mathbb{R}^2$ we connect the two points by a line segment, obtaining

$$x(t; \alpha) = (1 - \alpha)x_1(t) + \alpha x_2(t), \quad 0 \leq \alpha \leq 1. \quad (24)$$

For $M = \mathbb{S}^2$, the linear connection between the two points does not exist on the sphere, and we therefore use the geodesic arc between $x_1(t)$ and $x_2(t)$ instead, again interpolating according to $\alpha \in [0, 1]$.

See the accompanying paper video for examples.

5 OBSERVER-RELATIVE QUANTITIES

We want to be able to interactively compute the observed input vector field \mathbf{v} and its derivatives, relative to the rigid motion described by \mathbf{w} . In terms of the observer \mathbf{w} given by the function $t \mapsto (a(t), b(t), c(t))$, below we will make use of the following expansions and derivatives,

$$\begin{aligned} \mathbf{w}(x, t) &= a(t) \mathbf{e}_1(x) + b(t) \mathbf{e}_2(x) + c(t) \mathbf{e}_3(x), \\ \nabla \mathbf{w}(x, t) &= a(t) \nabla \mathbf{e}_1(x) + b(t) \nabla \mathbf{e}_2(x) + c(t) \nabla \mathbf{e}_3(x), \\ \frac{\partial \mathbf{w}(x, t)}{\partial t} &= \frac{da(t)}{dt} \mathbf{e}_1(x) + \frac{db(t)}{dt} \mathbf{e}_2(x) + \frac{dc(t)}{dt} \mathbf{e}_3(x). \end{aligned} \quad (25)$$

5.1 Reference Frame Transformation

In order to transform between two reference frames, we define a time-dependent diffeomorphism $t \mapsto \phi_t$, with each diffeomorphism, for fixed t , mapping from M to M , i.e., $\phi_t : M \rightarrow M$. For physically-realizable observers, each diffeomorphism ϕ_t is in fact an *isometry*.

For $M = \mathbb{R}^2$, the isometry ϕ_t can be written explicitly as

$$\phi_t(x) = w(t) + \mathbf{Q}(t)(x - w(t_0)), \quad (26)$$

where $w(t_0)$ is some arbitrary position at $t = t_0$, and each $\mathbf{Q}(t)$ is a rotation tensor. In Cartesian coordinates, the rotation $\mathbf{Q}(t)$ is given by

$$\mathbf{Q}(t) = \begin{bmatrix} \cos \theta(t) & -\sin \theta(t) \\ \sin \theta(t) & \cos \theta(t) \end{bmatrix}. \quad (27)$$

The path $t \mapsto w(t)$ and the integrated angle $\theta(t)$ are the solutions of

$$\frac{d}{dt} w(t) = \mathbf{w}(w(t), t), \quad \frac{d}{dt} \theta(t) = c(t), \quad (28)$$

with $\theta(t_0) = 0$. We can solve these two ODEs explicitly by

$$w(t) = w(t_0) + \int_{t_0}^t \mathbf{w}(w(\tau), \tau) d\tau, \quad \theta(t) = \int_{t_0}^t c(\tau) d\tau. \quad (29)$$

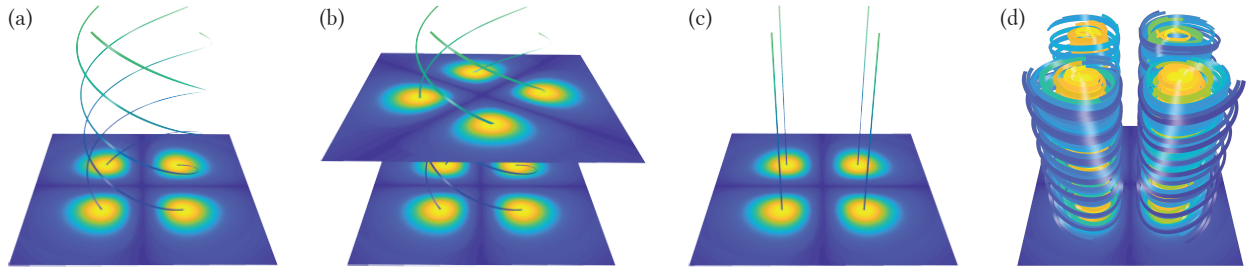


Fig. 7. **Four centers.** (a,b) LAVD [21] and λ_2 vortex core lines agree (vertical axis is time). (c) Vortex core lines observed relative to an observer \mathbf{w} selected from an observer field \mathbf{u} computed via optimization [18]. (d) Observed path lines swirling around the core lines using variance color-coding.

To transform vectors and tensors with the diffeomorphism ϕ_t , we use the pullback ϕ_t^* . On $M = \mathbb{R}^2$, the pullback $\phi_t^* \mathbf{x}$ of a vector field \mathbf{x} is

$$\phi_t^* \mathbf{x} = \mathbf{Q}^T(t) \mathbf{x}. \quad (30)$$

The pullback $\phi_t^* \mathbf{T}$ of a second-order tensor field \mathbf{T} (a linear map) is

$$\phi_t^* \mathbf{T} = \mathbf{Q}^T(t) \mathbf{T} \mathbf{Q}(t). \quad (31)$$

For details on diffeomorphisms and pullbacks, and explicit formulas for $M = \mathbb{S}^2$, we refer to Appendixes D and E (supplementary material).

5.2 Observed Velocity

The observed velocity, with respect to the observer \mathbf{w} , is obtained as

$$\mathbf{v}^* = \phi_t^* (\mathbf{v} - \mathbf{w}). \quad (32)$$

This velocity is of particular importance for vortex detectors that search for critical points of the velocity field, i.e., in this case the critical points of \mathbf{v}^* . In terms of the observer \mathbf{w} as $t \mapsto (a(t), b(t), c(t))$, this becomes

$$\mathbf{v}^* = \phi_t^* (\mathbf{v} - a(t) \mathbf{e}_1 - b(t) \mathbf{e}_2 - c(t) \mathbf{e}_3). \quad (33)$$

5.3 Observed Velocity Gradient

The observed velocity gradient, with respect to the observer \mathbf{w} , is

$$\nabla \mathbf{v}^* = \phi_t^* (\nabla \mathbf{v} - \nabla \mathbf{w}). \quad (34)$$

This velocity gradient is of particular importance for all vortex detectors that compute its eigenvalues and determine vortex-like behavior only when there are complex eigenvalues (2D: one conjugate complex pair). For these criteria, the relevant eigenvalues are therefore those of $\nabla \mathbf{v}^*$. In terms of the observer \mathbf{w} as $t \mapsto (a(t), b(t), c(t))$, this becomes

$$\nabla \mathbf{v}^* = \phi_t^* \left(\nabla \mathbf{v} - a(t) \nabla \mathbf{e}_1 - b(t) \nabla \mathbf{e}_2 - c(t) \nabla \mathbf{e}_3 \right). \quad (35)$$

5.4 Observed Time Derivative

The observed time derivative [18, 39], with respect to the observer \mathbf{w} , is

$$\begin{aligned} \frac{\partial \mathbf{v}^*}{\partial t} &= \phi_t^* \left(\frac{\mathcal{D}}{\mathcal{D}t} (\mathbf{v} - \mathbf{w}) \right), \\ &= \phi_t^* \left(\frac{\partial \mathbf{v}}{\partial t} - \frac{\partial \mathbf{w}}{\partial t} + \nabla \mathbf{v}(\mathbf{w}) - \nabla \mathbf{w}(\mathbf{v}) \right). \end{aligned} \quad (36)$$

In terms of the observer \mathbf{w} as $t \mapsto (a(t), b(t), c(t))$, this becomes

$$\begin{aligned} \frac{\partial \mathbf{v}^*}{\partial t} &= \phi_t^* \left(\frac{\partial \mathbf{v}}{\partial t} - \frac{da(t)}{dt} \mathbf{e}_1 - \frac{db(t)}{dt} \mathbf{e}_2 - \frac{dc(t)}{dt} \mathbf{e}_3 + \right. \\ &\quad \left. \nabla \mathbf{v}(a(t) \mathbf{e}_1 + b(t) \mathbf{e}_2 + c(t) \mathbf{e}_3) - \right. \\ &\quad \left. (a(t) \nabla \mathbf{e}_1 + b(t) \nabla \mathbf{e}_2 + c(t) \nabla \mathbf{e}_3) \mathbf{v} \right). \end{aligned} \quad (37)$$

See Appendix F (supplementary material) and previous work [18, 39] for more on observed time derivatives. In addition, we give equations for the *observed acceleration* in Appendix G (supplementary material).

6 DETERMINING OBSERVERS FROM PRIOR METHODS

We now demonstrate the generality and versatility of our framework by describing how observers can be defined via (1) Extraction from a globally optimized, continuous field of observers [18, 39]; (2) Extraction from separate observers optimized at each space-time point [14]; (3) Replication of Lagrangian-Averaged Vorticity Deviation (LAVD) [21] in our framework, relative to a special objectively-determined observer.

6.1 Observer Fields from Global Optimization

A directly suitable choice for the observer field \mathbf{u} required by our framework are the observer fields computed by global optimization methods in the plane [18], or on the sphere [39], respectively. We have used this approach in the results shown in Fig. 4, Fig. 7, and Fig. 9.

6.2 Observer Fields from Generic Objective Vortices

In order to obtain a valid observer field from the *generic objective vortices* method of Günther et al. [14], we first use their optimization method to compute an optimal, objective field $\bar{\mathbf{v}}$ (Eq. 20 in [14]). From the objective field $\bar{\mathbf{v}}$, we then compute a smooth observer field \mathbf{u} as

$$\mathbf{u} := \mathbf{v} - \bar{\mathbf{v}}. \quad (38)$$

This simple approach allows us to directly use the objective optimization method of Günther et al. [14] as an input to our framework. We have computed the observer field used in Fig. 1 with this approach.

We note that the above approach is objective and can indeed be used to obtain a valid observer field \mathbf{u} , despite the fact that the optimization [14] computes a *different* observer for each point in space-time. Since the objective vector field $\bar{\mathbf{v}}$ is defined at each space-time point, the observer field obtained via Eq. 38 describes valid, smooth observer motions. In fact, these motions are *determined objectively*, because the vector $\bar{\mathbf{v}}$ at each point in space-time is objective [14], and thus the corresponding velocities \mathbf{u} are determined objectively. The obtained field \mathbf{u} then enables the extraction of observers using our framework. We note, however, that, in general, we do not extract the exact same observers that are used for vortex detection in [14], because the derivatives given in [14] do not correspond to the field \mathbf{u} that we obtain via Eq. 38.

6.3 Observers for Lagrangian-Averaged Vorticity Deviation

Our framework can be used to compute results equivalent to the LAVD method by Haller et al. [21], in the following way. See Fig. 7.

We define an observer \mathbf{w} , for $M = \mathbb{R}^2$, via $t \mapsto (a(t), b(t), c(t))$, by setting $a(t) = b(t) = 0$, and defining $c(t) := \bar{\omega}(t)$. Here, we set the angular velocity $\bar{\omega}(t)$ to half the average vorticity magnitude⁴ of a chosen region $U(t) \subset \mathbb{R}^2$ of the flow field \mathbf{v} , as defined by Haller et al. [21]. As Haller et al., we assume that the region $U(t)$ is invariant under the flow of \mathbf{v} , i.e., the region is deformed over time by the flow (map) of \mathbf{v} . We can then obtain the same scalar field as the LAVD field defined by Haller et al. [21], by simply integrating the *observed vorticity magnitude*, as observed by the observer \mathbf{w} , along path lines of the field \mathbf{v} in the same region $U(t)$ used for computing $\bar{\omega}(t)$. We can

⁴We note that the different definitions of angular velocity, vorticity (curl), and the vorticity tensor, require divisions or multiplications by two for conversion.

obtain the observed vorticity from the *observed velocity gradient* $\nabla \mathbf{v}^*$ (Sec. 5.3), given by Eqs. 34, 35, giving the observed vorticity tensor as

$$\boldsymbol{\Omega}^* = \frac{1}{2} \left(\nabla \mathbf{v}^* - (\nabla \mathbf{v}^*)^T \right). \quad (39)$$

We note that due to our definition of the observer \mathbf{w} , the observed vorticity magnitude is identical to the instantaneous vorticity deviation (IVD) of Haller et al. [21], and therefore its integral along path lines is identical to LAVD. However, we do not need to explicitly compute the deviation of vorticity from the average vorticity, as Haller et al. [21] do: The vorticity that we integrate is simply the regular vorticity magnitude observed by \mathbf{w} . Nevertheless, the resulting LAVD scalar field is the same, because the observer \mathbf{w} is rotating with the average angular velocity $\bar{\omega}(t)$, as defined by Haller et al. [21]. In this way, we gain additional insight into the meaning of LAVD: It is, in fact, the (integrated) vorticity magnitude seen by a particular, objectively-determined observer.

Averaging observers. We can gain even more insight from the following formulation: Given the region $U(t)$, we extract an observer from the field $\mathbf{u} := \mathbf{v}$ at every point $x \in U(t)$, for fixed t , obtaining a function $t \mapsto (a_i(t), b_i(t), c_i(t))$ for each $i = x$. We then define the *average observer* $\bar{\mathbf{w}}$ over $U(t)$ via Eq. 22, i.e., we average (a_i, b_i, c_i) , over all $i = x \in U(t)$ to obtain $t \mapsto (\bar{a}(t), \bar{b}(t), \bar{c}(t))$. If we project this average observer to $t \mapsto (0, 0, \bar{c}(t))$, this is the same observer that we defined above via the average angular velocity $\bar{\omega}(t)$. IVD and LAVD can thus be formulated using the average observer of the region $U(t)$, followed by an appropriate projection. For our basis fields $\{\mathbf{e}_1, \mathbf{e}_2, \mathbf{e}_3\}$, $\bar{c}\mathbf{e}_3$ contains the entire vorticity. We can thus either project to \mathbf{e}_3 , or notice that Eq. 39 is, in fact, independent of \mathbf{e}_1 and \mathbf{e}_2 (see Eq. 9).

7 IMPLEMENTATION AND PERFORMANCE

We have implemented our framework for interactive observer-relative visualization in C++ and OpenGL.

7.1 Reference Frame Transformation

There are two major ways for the transformation of path lines of a vector field from a given observer to another observer:

1. Transform the vector field, using Eq. 32, and integrate path lines using the standard approach in the transformed vector field.
2. Transform the geometry (vertices) of path lines computed for one observer to another observer, directly using the frame transformation given by the time-dependent diffeomorphism ϕ_t .

For best interactivity, for path lines we use the second approach above:

We first compute a set of path lines for the lab frame observer, storing each path line as a vertex sequence $[p_1, p_2, \dots, p_k]$. In order to display the same path lines relative to any other observer, we simply individually transform the spatial position of each vertex: For each vertex p_i , we obtain the transformed vertex via the inverse of the diffeomorphism ϕ_t given by Eq. 26, i.e.,

$$p_i^* = \phi_t^{-1}(p_i), \quad \text{with } t = t(i). \quad (40)$$

For $M = \mathbb{R}^2$, this is simply applying a rotation and a translation, for each given time t . However, since each vertex p_i on the path line corresponds to a different time t , each vertex must be transformed with the map ϕ_t^{-1} for a different time parameter t , which here we refer to as $t(i)$, i.e., the time parameter corresponding to vertex number i . See Fig. 8 for an example for 1,200 path lines seeded on a regular grid.

For $M = \mathbb{S}^2$, we do the same with the map ϕ_t given in Appendix E.

7.2 Performance

Table 1 shows performance on a dual Intel Xeon 6230R (52 cores) and an NVIDIA GeForce RTX 3090. We first integrate path lines for the lab frame on the CPU, parallelized over all CPU cores, and then store the resulting vertex array on the GPU. Table 1 (left) shows computation times and overall throughput of vertices computed per second. When integrating enough path lines in parallel we achieve more than 15M vertices per second. For each time step, we typically compute two to

Table 1. **Performance.** Left half: path line integration, vertex throughput. Right half: observer world line integration, sample throughput.

data set	# path lines	time [ms]	vtxs per s	# point samples	time [ms]	samples per s
Four centers	64	26	15 M	6.28×10^2	6	100 K
	256	83	19 M	6.28×10^3	12	509 K
	1,024	238	27 M	6.28×10^4	87	723 K
Boussinesq	64	23	14 M	5×10^2	13	38 K
	256	76	17 M	5×10^3	21	234 K
	1,024	293	17 M	5×10^4	82	609 K

ten vertices. Every time the observer changes, we compute Eq. 29 on the CPU, transfer the result to the GPU, and apply Eq. 40 to each vertex in a vertex shader. Table 1 (right) shows the throughput of samples along the observer world line. Overall, our system is fully interactive and achieves 20–30 frames per second for observed path line rendering. Performance mainly depends on the number of computed path lines and the corresponding number of vertices, and not on the data set. See Appendix H and I in the supplementary material for more details.

8 RESULTS

We demonstrate different aspects of our framework on analytically defined test cases, and on numerically-simulated flow fields.

Cylinder flow (Fig. 6). The vortices behind a cylinder [27] in this data set are short-lived, and new vortices develop periodically. We demonstrate that a moving observer helps to produce a less obstructed view of the individual vortices, using an observer given by a constant velocity (translation). The vertical axis and the color map encode time in this example. By animating the observer's translation, we provide a visual clue how the data observed in the lab frame is transformed into the frame of a moving observer. The transition between the lab frame and the final observer results from direct interpolation (Sec. 4.2).

Vortex street (cylinder) (Fig. 8). This numerical simulation of a vortex street behind a cylindrical obstacle is an example for a flow field that is easier to interpret in a moving reference frame. Unlike other examples, here we have not computed an observer, but show that simply extracting an observer from the ambient flow of the input field \mathbf{v} is enough to define a suitable observer. Fig. 8 shows snapshots of the interpolation between lab frame visualization (top) to the co-moving observer (bottom). We point out that, although the observer was extracted along a path line in the input flow, our framework guarantees that each individual frame of the sequence corresponds to a physically-observable visualization, relative to a physically-realizable observer.

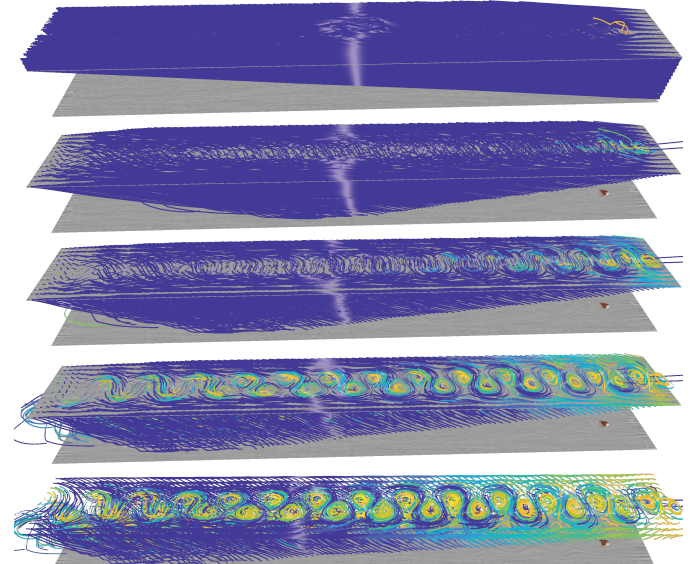


Fig. 8. **Vortex street (cylinder).** Changing the observer interactively (top to bottom) allows revealing the vortices (bottom) obstructed in the lab frame (top). (The vertical axis in each visualization corresponds to time.)

We automatically compute a color-coding based on the *variance* of the spatial locations (relative to the chosen observer) of a particle over time, along its path line. This highlights the centers of vortices, provided that the chosen observer perceives the particle as swirling around a mostly static center. Low variance is mapped to brighter hues in the color map. This effect is clearly visible in Fig. 8 (bottom).

Bickley jet (Fig. 9). This data set [21] contains an analytically-defined vortex street. Relative to a moving observer, the vortex structures become clearly visible. We compute the observer field \mathbf{u} via global optimization [18]. Fig. 9(a) shows path lines in the lab frame, Fig. 9(b) shows observed path lines. We keep the color for each path line constant (minimum observed variance) for the transformation sequence (Fig. 9(a) to (b)). This demonstrates that color-coding is not enough to show the vortex structures. The transformation of the pathlines achieves a better visualization.

Four centers (Fig. 7). This data set by Günther et al. [15] contains four centers that rotate around a common axis. We show that LAVD [21] (color-coded) detects these four vortices, and compare LAVD with vortex core lines computed with the λ_2 criterion [24]. Figs. 7(a,b) show that LAVD and the λ_2 vortex cores agree. Fig. 7(c) shows the observed vortex core lines relative to an observer that rotates along with the vortices. We have computed this observer via global optimization [18]: The observed vortex core lines stay in place. In this reference frame, it is now trivial to verify that path lines seeded around the centers swirl around the vortex cores (Fig. 7(d)). The color coding of the swirling path lines in Fig. 7(d) is computed according to path line variance.

Beads flow (Fig. 5(a,b)). This flow was originally given by Wiebel et al. [51]. We use the analytic version used by Weinkauf and Theisel [49] and by Günther et al. [15]. It contains a contracting flow (a sink) that rotates around a center as observed by the input lab frame. Fig. 5(a) shows the input flow field, relative to the lab frame. Fig. 5(b) shows the flow relative to an observer that rotates with constant angular velocity, computed via optimization [18]. We see that all observed path lines are now straight lines (depicted as “shadows”) that converge at the same point. Moreover, using our framework we have found that all observers extracted from the input field \mathbf{v} perceive this flow field without any rotational motion. They are, in fact, all rotating with the same angular velocity. Since we have objectively determined observers that perceive this flow without any rotational motion, we must conclude that all observed rotation in this flow is solely due to the rotation of a reference frame, and the flow itself does not contain intrinsic rotational motion. (We note, however, that this is a purely *kinematic* judgement. In terms of *dynamics*, a rotating frame and an inertial frame behave differently.)

Divergence-free beads flow (Fig. 5(c,d)). This field is a modification of the original beads flow to make it divergence-free, used by Günther et al. [15] as a test case for rotation-invariant vortex detection. Using interactive observer exploration, we can see that the input flow in Fig. 5(c) is in fact itself a Killing field: We choose $\mathbf{u} := \mathbf{v}$, and interactively see that all observers extracted from this observer field are in fact the same observer, as can also be confirmed via Eq. 14, and that the observer-relative visualization shows no motion at all. The observed field is identically zero, as shown in Fig. 5(d). We view this

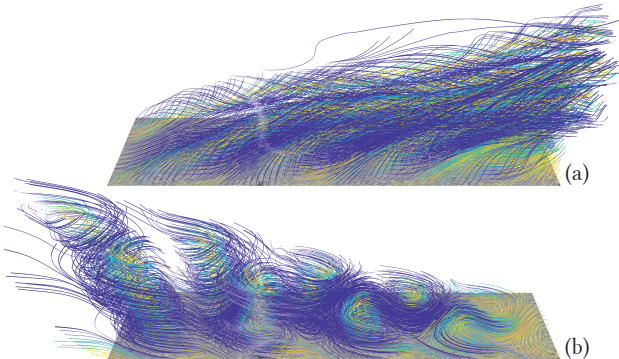


Fig. 9. **Bickley jet.** The input lab frame obstructs the visibility of vortices (a). A globally optimized observer [18] reveals the vortices clearly (b). (The vertical axis in each visualization corresponds to time.)

field as an example of “if the motion described by a vector field is purely an observer motion, then the input field contains no intrinsic motion.” The same is confirmed by an observer field computed via global optimization [18]: The optimized observer field \mathbf{u} is $\mathbf{u} = \mathbf{v}$.

A fundamental problem with detecting a vortex in this data set is that, since the field can be observed as the 0-field, *any rotating observer can be used in order to perceive a vortex at any chosen location*. We suggest that the only consistent interpretation is that there is in fact no objective vortex contained in this field, unless one chooses to detect vortices with respect to a non-objectively chosen, special observer.

Vortex on the sphere (Fig. 4). To demonstrate that our framework is also applicable to spherical domains, we illustrate a result for a flow field with a synthetic vortex moving once around a sphere. Path lines observed relative to the lab frame are hard to interpret since they move once around the sphere, as shown in Fig. 4 (left). From left to right, Fig. 4 shows snapshots from the observer transformation between the lab frame and a globally optimized observer [39] that moves with the vortex. The last frame in the sequence clearly shows the “steady” vortex that is observed by the objectively-determined, moving observer.

Boussinesq (Fig. 1). This is a more complex scenario that requires interactive exploration of the input flow field shown in Fig. 1(a). We first use the objective optimization method by Günther et al. [14], obtaining an observer field as described in Sec. 6.2. We then visualize the flow relative to one physically-realizable observer at a time, but smoothly transition between a large number of observers: As shown in the accompanying video, we interactively move the location where an observer is extracted from the observer field. Fig. 1(e) depicts six different observer-relative visualizations. We modulate the opacity of each path line with its variance; path lines with high variance become fully transparent, making vortex structures fade in and out while the observer is being changed, as demonstrated in the video.

Figs. 1(b-d) show tools to help guide the exploration of the vast space of possible observers. Fig. 1(b) shows possible vortex core positions computed via the λ_2 criterion, which can help in finding good observers. Fig. 1(c) depicts color-coded observer similarity (Eq. 14), which can help identify observers that are significantly different from the current observer. Fig. 1(d) shows the (a, b, c) parameter space of linear velocity (horizontal) and vorticity (vertical; positive in red, negative in blue). This provides further insight into the space of possible observers: Each observer is a curve in the 3D parameter space (left subimage); the six observers from Fig. 1(e) correspond to six curves (right subimage).

9 CONCLUSIONS

Our framework demonstrates that in order to reveal vortex structures in flow fields where one reference frame cannot depict all features simultaneously, interactive exploration of the space of observers is beneficial or might even be necessary. Our framework is flexible enough to incorporate observers that are objectively computed with several different available state-of-the-art methods. In contrast to prior work computing features jointly, we focus on individual, physically-realizable observers for visualization and vortex detection. We believe that our framework can provide a common basis for the future investigation of the interaction between feature detectors derived using physical arguments on the one hand, and the flexible definition of observer fields on the other.

Determining observers objectively can be crucial. For example, our exploration of the beads flow has shown that when observers are not chosen objectively, the perceived rotation can be due solely to the choice of observer: Rotation can be detected where there is no intrinsic (kinematic) rotation. However, we have also illustrated several *different* ways of choosing observers objectively. We therefore believe that further investigation of the meaning and implications of objective vortex detection and objectively determining observers is necessary, and we hope that our framework can contribute in this endeavor.

ACKNOWLEDGMENTS

We thank Anna Frühstück for help with the figures and the video. This work was supported by King Abdullah University of Science and Technology (KAUST). This research used resources of the Core Labs of King Abdullah University of Science and Technology.

REFERENCES

- [1] G. Astarita. Objective and generally applicable criteria for flow classification. *Journal of Non-Newtonian Fluid Mechanics*, 6(1):69–76, 1979.
- [2] O. Azencot, M. Ben-Chen, F. Chazal, and M. Ovsjanikov. An operator approach to tangent vector field processing. *Computer Graphics Forum*, 32(5):73–82, 2013.
- [3] O. Azencot, M. Ovsjanikov, F. Chazal, and M. Ben-Chen. Discrete derivatives of vector fields on surfaces—an operator approach. *ACM Transactions on Graphics*, 34(3):Article No. 29, 2015.
- [4] I. Baeza Rojo and T. Günther. Vector field topology of time-dependent flows in a steady reference frame. *IEEE Transactions on Visualization and Computer Graphics*, 26(1):280–290, 2020.
- [5] D. C. Banks and B. A. Singer. A predictor-corrector technique for visualizing unsteady flow. *IEEE Transactions on Visualization and Computer Graphics*, 1(2):151–163, 1995.
- [6] M. Ben-Chen, A. Butscher, J. Solomon, and L. Guibas. On discrete Killing vector fields and patterns on surfaces. In *Proceedings of Eurographics Symposium on Geometry Processing*, pp. 1701–1711, 2010.
- [7] R. Bujack, M. Hlawitschka, and K. I. Joy. Topology-inspired Galilean invariant vector field analysis. In *Proceedings of IEEE Pacific Visualization 2016*, pp. 72–79, 2016.
- [8] B. Cabral and L. C. Leedom. Imaging vector fields using line integral convolution. In *Proceedings of SIGGRAPH ’93*, pp. 263–270, 1993.
- [9] M. P. do Carmo. *Riemannian Geometry*. Birkhäuser, 1992.
- [10] E. Dresselhaus and M. Tabor. The kinematics of stretching and alignment of material elements in general flow fields. *Journal of Fluid Mechanics*, 236:415–444, 1991.
- [11] R. Drouot and M. Lucius. Approximation du second ordre de la loi de comportement des fluides simples. Lois classiques déduites de l’introduction d’un nouveau tenseur objectif. *Archiwum Mechaniki Stosowanej*, 28(2):189–198, 1976.
- [12] T. Frankel. *The Geometry of Physics: An Introduction*. Cambridge University Press, 3rd ed., 2011.
- [13] C. Garth, X. Tricoche, T. Salzbrunn, T. Bobach, and G. Scheuermann. Surface techniques for vortex visualization. In *Proceedings of Eurographics/IEEE VGTC Symposium on Visualization*, pp. 155–164, 2004.
- [14] T. Günther, M. Gross, and H. Theisel. Generic objective vortices for flow visualization. *ACM Transactions on Graphics*, 36(4):Article No. 141, 2017.
- [15] T. Günther, M. Schulze, and H. Theisel. Rotation invariant vortices for flow visualization. *IEEE Transactions on Visualization and Computer Graphics*, 22(1):817–826, 2016.
- [16] T. Günther and H. Theisel. Hyper-objective vortices. *IEEE Transactions on Visualization and Computer Graphics*, 25(1):1–1, 2018.
- [17] T. Günther and H. Theisel. The State of the Art in Vortex Extraction. *Computer Graphics Forum*, 37(6):149–173, 2018.
- [18] M. Hadwiger, M. Mlejnek, T. Theußl, and P. Rautek. Time-dependent flow seen through approximate observer Killing fields. *IEEE Transactions on Visualization and Computer Graphics*, 25(1):1257–1266, 2019.
- [19] G. Haller. An objective definition of a vortex. *Journal of Fluid Mechanics*, 525:1–26, 2005.
- [20] G. Haller. Can vortex criteria be objectivized? *Journal of Fluid Mechanics*, 508:A25, 2021.
- [21] G. Haller, A. Hadjighasem, M. Farazmand, and F. Huhn. Defining coherent vortices objectively from the vorticity. *Journal of Fluid Mechanics*, 795:136–173, 2016.
- [22] G. A. Holzapfel. *Nonlinear Solid Mechanics: A Continuum Approach for Engineering*. Wiley, 2000.
- [23] J. C. R. Hunt, A. A. Wray, and P. Moin. Eddies, streams, and convergence zones in turbulent flows. In *Proceedings of the Summer Program 1988*, pp. 193–208. Center for Turbulence Research, Dec. 1988.
- [24] J. Jeong and F. Hussain. On the identification of a vortex. *Journal of Fluid Mechanics*, 285:69–94, 1995.
- [25] B. Jobard, G. Erlebacher, and M. Y. Hussaini. Lagrangian-Eulerian advection of noise and dye textures for unsteady flow visualization. *IEEE Transactions on Visualization and Computer Graphics*, 8(3):211–222, 2002.
- [26] B. Jobard and W. Lefer. Creating evenly-spaced streamlines of arbitrary density. In *8th Eurographics Workshop on Visualization in Scientific Computing*, pp. 211–222, 1997.
- [27] C. Jung, T. Tél, and E. Ziemniak. Application of scattering chaos to particle transport in a hydrodynamical flow. *Chaos: An Interdisciplinary Journal of Nonlinear Science*, 3(4):555–568, 1993.
- [28] M. Kilian, N. J. Mitra, and H. Pottmann. Geometric modeling in shape space. *ACM Transactions on Graphics*, 26(3):Article No. 64, 2007.
- [29] H. J. Lugt. The dilemma of defining a vortex. In *Recent Developments in Theoretical and Experimental Fluid Mechanics: Compressible and Incompressible Flows*, pp. 309–321. Springer-Verlag, 1979.
- [30] J. E. Marsden and T. J. Hughes. *Mathematical Foundations of Elasticity*. Dover Publications, Inc., 1994.
- [31] J. Martinez Esturo, C. Rössl, and H. Theisel. Generalized metric energies for continuous shape deformation. In *Mathematical Methods for Curves and Surfaces*, Lecture Notes in Computer Science, pp. 135–157. Springer-Verlag, 2012.
- [32] A. McInerney. *First Steps in Differential Geometry*. Springer-Verlag, 2013.
- [33] R. W. Ogden. *Non-Linear Elastic Deformations*. Dover Publications, Inc., 1997.
- [34] A. Okubo. Horizontal dispersion of floatable particles in the vicinity of velocity singularities such as convergences. *Deep Sea Research and Oceanographic Abstracts*, 17(3):445–454, June 1970.
- [35] R. Peikert and M. Roth. The “Parallel Vectors” operator—a vector field visualization primitive. In *Proceedings of IEEE Visualization ’99*, pp. 263–262, 1999.
- [36] A. E. Perry and M. S. Chong. A description of eddying motions and flow patterns using critical-point concepts. *Ann. Rev. Fluid Mech.*, 19(1):125–155, 1987.
- [37] A. E. Perry and M. S. Chong. Topology of flow patterns in vortex motions and turbulence. *Applied Scientific Research*, 53(3):357–374, 1994.
- [38] P. Petersen. *Riemannian Geometry*. Springer-Verlag, 3rd ed., 2016.
- [39] P. Rautek, M. Mlejnek, J. Beyer, J. Troidl, H. Pfister, T. Theußl, and M. Hadwiger. Objective observer-relative flow visualization in curved spaces for unsteady 2d geophysical flows. *IEEE Transactions on Visualization and Computer Graphics*, 27(2):283–293, 2021.
- [40] S. K. Robinson. A review of vortex structures and associated coherent motions in turbulent boundary layers. In *Proceedings of Structure of Turbulence and Drag Reduction, IUTAM Symposium*, pp. 23–50. Springer-Verlag, 1990.
- [41] P. G. Saffman. *Vortex Dynamics*. Cambridge University Press, 1995.
- [42] J. Sahner, T. Weinkauf, and H.-C. Hege. Galilean invariant extraction and iconic representation of vortex core lines. In *Proceedings of Eurographics/IEEE VGTC Symposium on Visualization*, pp. 151–160, 2005.
- [43] J. Solomon, M. Ben-Chen, A. Butscher, and L. Guibas. As-Killing-as-possible vector fields for planar deformation. In *Proceedings of Eurographics Symposium on Geometry Processing*, pp. 1543–1552, 2011.
- [44] D. Sujudi and R. Haimes. Identification of swirling flow in 3-d vector fields. In *Proceedings of the 12th Computational Fluid Dynamics Conference*, pp. 792–799, 1995.
- [45] H. Theisel, M. Hadwiger, P. Rautek, T. Theußl, and T. Günther. Vortex criteria can be objectivized by unsteadiness minimization. arXiv:2106.16169 [physics.flu-dyn], 2021.
- [46] C. Truesdell and W. Noll. *The Nonlinear Field Theories of Mechanics*. Springer-Verlag, 1965.
- [47] J. J. van Wijk. Image based flow visualization. *ACM Transactions on Graphics*, 21(3):745–754, 2002.
- [48] T. Weinkauf, J. Sahner, H. Theisel, and H.-C. Hege. Cores of swirling particle motion in unsteady flows. *IEEE Transactions on Visualization and Computer Graphics*, 13(6):1759–1766, 2007.
- [49] T. Weinkauf and H. Theisel. Streak lines as tangent curves of a derived vector field. *IEEE Transactions on Visualization and Computer Graphics*, 16(6):1225–1234, 2010.
- [50] J. Weiss. The dynamics of enstrophy transfer in two-dimensional hydrodynamics. *Physica D: Nonlinear Phenomena*, 48(2):273–294, Mar. 1991.
- [51] A. Wiebel, R. Chan, C. Wolf, A. Robitzki, A. Stevens, and G. Scheuermann. Topological flow structures in a mathematical model for rotation-mediated cell aggregation. In *Topological Methods in Data Analysis and Visualization, Mathematics and Visualization*, pp. 193–204, 2009.

A THE LIE ALGEBRA OF OBSERVER MOTIONS

A Lie algebra is a vector space with an additional vector product, the so-called Lie bracket. In our context, we model any possible physically-realizable observer motion as an element (in terms of the vector space structure, a “vector”) of the corresponding Lie algebra. This Lie algebra therefore comprises all possible observer motions. However, in our framework each Lie algebra element is in fact a whole (Killing) vector field \mathbf{w} on the underlying manifold M , where M constitutes the domain where the input vector field as well as any Killing field describing observer motion are given. In this paper, $M = \mathbb{R}^2$ or $M = \mathbb{S}^2$.

The vector space structure means that a Lie algebra has a basis, i.e., a spanning set of n linearly-independent basis vectors (basis vector fields) for an n -dimensional Lie algebra. The Lie algebras of rigid motions for the manifolds $M = \mathbb{R}^2$ and $M = \mathbb{S}^2$, respectively, are each three-dimensional as a vector space. This implies that any element of the Lie algebra, i.e., any rigid motion, can be referred to three basis vectors (here, basis vector fields), giving three corresponding real coefficients:

$$\mathbf{w}(x, t) = a(t)\mathbf{e}_1(x) + b(t)\mathbf{e}_2(x) + c(t)\mathbf{e}_3(x). \quad (41)$$

This expression is a linear combination of three basis vector fields with three real coefficients (a, b, c) . (One triplet $(a(t), b(t), c(t))$ per time t .)

Scalar multiplication: Scalar times Lie algebra element

The scalar multiplication for the vector space structure, e.g., $a\mathbf{e}_1$, where \mathbf{e}_1 denotes a vector field on M , is defined pointwise in each tangent space via standard scalar multiplication in the tangent space:

$$(a\mathbf{e}_1)(x) := a\mathbf{e}_1(x). \quad (42)$$

That is, in each tangent space $T_x M$ at a point $x \in M$, the basis vector in that tangent space, i.e., $\mathbf{e}_1(x)$, is multiplied by the same coefficient a .

Vector addition: Addition of two Lie algebra elements

Likewise, the vector addition for the vector space structure is also defined by pointwise addition of vectors in each tangent space:

$$(\mathbf{e}_1 + \mathbf{e}_2)(x) := \mathbf{e}_1(x) + \mathbf{e}_2(x). \quad (43)$$

Linear independence of the Lie algebra basis

It is important to realize that the linear independence of our Lie algebra basis needs to be verified as the linear independence of vector fields, not as that for individual vectors in some tangent space. (Otherwise, in a two-dimensional tangent space more than two vectors would always be linearly dependent; but we have three linearly independent basis vector fields.) That is, linear independence of three basis fields $\mathbf{e}_i, \mathbf{e}_j, \mathbf{e}_k$ is given if there are no coefficients $\lambda, \mu \in \mathbb{R}$ such that

$$\mathbf{e}_i = \lambda\mathbf{e}_j + \mu\mathbf{e}_k. \quad (44)$$

for every (cyclic) permutation of $(i, j, k) = (1, 2, 3)$. This equation must be read such that for fixed $\lambda, \mu \in \mathbb{R}$, for all points $x \in M$, the vectors in each tangent space $T_x M$ would have to be

$$\mathbf{e}_i(x) = \lambda\mathbf{e}_j(x) + \mu\mathbf{e}_k(x). \quad (45)$$

In our framework, for $M = \mathbb{R}^2$ and the basis given by Eq. 8, this is trivial to see for $\mathbf{e}_i = \mathbf{e}_3$. However, it is also not hard to see in the other cases. For $M = \mathbb{S}^2$ and the basis given by Eq. 11, we can imagine choosing two basis fields to reproduce a non-zero vector of the third basis field at some point, and then considering the “pole” of the third field, where the third field has a critical point (the vector is zero), but the linear combination that we just considered gives a non-zero vector.

Time dependence

While above we have considered the individual scalar multiplications, vector (field) additions, and linear independence, neglecting the time-dependence of vector fields on M , i.e., we have mainly considered

$$\mathbf{w}(x) = a\mathbf{e}_1(x) + b\mathbf{e}_2(x) + c\mathbf{e}_3(x), \quad (46)$$

everything trivially extends to time-dependent Killing fields with time-dependent coefficients $t \mapsto (a(t), b(t), c(t))$, giving Eq. 41 above.

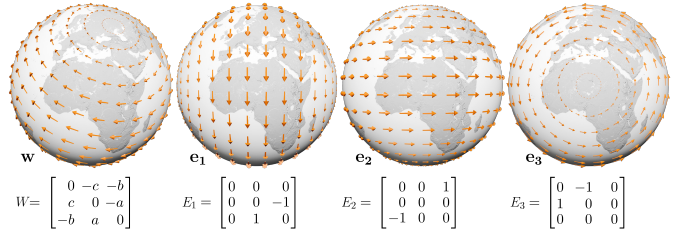


Fig. 10. **Physically-realizable observer motions referred to basis Killing fields on the sphere.** The Lie algebra of physically-realizable observer motions on the sphere is a three-dimensional vector space, where each element w can be referred to a basis of three linearly-independent basis Killing vector fields $\{\mathbf{e}_1, \mathbf{e}_2, \mathbf{e}_3\}$, such as those shown here (right).

The Lie bracket

The Lie bracket is a “vector multiplication” operation defined for a pair of vectors (elements) of a Lie algebra. In our case, these elements are vector fields, and the corresponding Lie bracket is then a map

$$[\cdot, \cdot]: \mathcal{X}(M) \times \mathcal{X}(M) \rightarrow \mathcal{X}(M), \quad (\mathbf{u}, \mathbf{v}) \mapsto [\mathbf{u}, \mathbf{v}]. \quad (47)$$

Here, $\mathcal{X}(M)$ denotes the space of all possible (smooth) vector fields on the manifold M . This Lie bracket of vector fields is a differential-geometric operator that maps a pair of vector fields on M to another vector field on M . Importantly, if we consider only the Killing vector fields on M , the Lie bracket maps a pair of Killing fields on M to another Killing field on M . The Lie bracket is identical to the Lie derivative of one vector field with respect to the flow of another vector field, i.e.,

$$[\mathbf{u}, \mathbf{v}] = \mathcal{L}_{\mathbf{u}} \mathbf{v}, \quad (48)$$

with both sides denoting a vector field. More explicitly, we can compute the vector field $\mathcal{L}_{\mathbf{u}} \mathbf{v}$, and thus the Lie bracket $[\mathbf{u}, \mathbf{v}]$, by

$$[\mathbf{u}, \mathbf{v}] = \mathcal{L}_{\mathbf{u}} \mathbf{v} = \nabla_{\mathbf{v}}(\mathbf{u}) - \nabla_{\mathbf{u}}(\mathbf{v}), \quad (49)$$

where $\nabla_{\mathbf{u}}$ and $\nabla_{\mathbf{v}}$ are the velocity gradient tensors of the vector fields \mathbf{u} and \mathbf{v} , respectively, and we evaluate in the directions \mathbf{v}, \mathbf{u} , respectively.

Observed time derivatives

The observed time derivative given in Eq. 36 is in fact a time-dependent Lie derivative. As such, it combines the autonomous Lie derivative, which is identical to the Lie bracket, with the partial time derivative of each field. We note that, similar to the Lie bracket, the time-dependent Lie derivative of a time-dependent Killing field with respect to another time-dependent Killing field is again a time-dependent Killing field.

Correspondence to matrix Lie groups

For completeness, we note that for Lie algebras of matrix Lie groups, the differential-geometric definition of the Lie bracket above can be substituted by the much simpler definition of the Lie bracket as a matrix commutator. In our context, for example, we can construct an isomorphism between the Lie algebra of all anti-symmetric 3×3 matrices (all “infinitesimal rotation matrices”) and the Lie algebra of all Killing vector fields on the sphere \mathbb{S}^2 . (A specific isomorphism can be constructed by choosing a particular basis for the space of all Killing fields, such as the basis given by Eq. 11. See Fig. 10.) Then, for two Killing fields $\mathbf{w}_1, \mathbf{w}_2$, and the corresponding anti-symmetric matrices W_1, W_2 , for coefficients $(a_1, b_1, c_1), (a_2, b_2, c_2)$, respectively, referring the Killing fields to the chosen basis $\{\mathbf{e}_1, \mathbf{e}_2, \mathbf{e}_3\}$, the Lie bracket operation can be computed simply as the matrix commutator

$$[W_1, W_2] = W_1 W_2 - W_2 W_1. \quad (50)$$

In this way, the vector field $[\mathbf{w}_1, \mathbf{w}_2]$ is the vector field corresponding to (via the isomorphism, i.e., the chosen basis) the matrix $[W_1, W_2]$.

Basis Killing fields on the sphere

Fig. 10 depicts the three basis Killing fields $\{\mathbf{e}_1, \mathbf{e}_2, \mathbf{e}_3\}$ on the sphere given by Eq. 11, and another Killing field \mathbf{w} as the linear combination with coefficients (a, b, c) referred to this basis. Below the spheres, the corresponding anti-symmetric matrices (see above) are shown.

Different basis Killing fields for the Euclidean plane

For illustration and completeness, we give another basis for all Killing fields on $M = \mathbb{R}^2$, different from the one defined in Eq. 8. In fact, any set of three vector fields $\{\mathbf{e}_1, \mathbf{e}_2, \mathbf{e}_3\}$, where each field is given by

$$\mathbf{e}_i(x, y) = \begin{bmatrix} 0 & -1 \\ 1 & 0 \end{bmatrix} \begin{bmatrix} x - x_0(i) \\ y - y_0(i) \end{bmatrix}, \quad \begin{bmatrix} x_0(i) \\ y_0(i) \end{bmatrix} \in \mathbb{R}^2, \quad i \in \{1, 2, 3\}, \quad (51)$$

is also a basis, provided that the three “center” points $(x_0(i), y_0(i))^T$ are chosen in general position, i.e., none of the points are at the same position, and no point lies on the line defined by the other two points.

Due to the different “centers” (i.e., critical points) of the basis vector fields, all three fields are linearly independent. They must therefore constitute a basis, even without checking anything else. Although this might be surprising, this implies that linear combinations of these three “rotational” basis fields can reproduce any constant-velocity vector field (it is not hard to confirm this explicitly), just like the basis fields given in Eq. 8 obviously can. However, then no single coefficient corresponds to angular velocity, unlike the coefficient c referred to the basis in Eq. 8. (For the basis in Eq. 51, the angular velocity is in fact $a + b + c$.)

B OBJECTIVITY AND OBJECTIVELY-DETERMINED OBSERVERS

We summarize important details, and highlight important subtleties, of the concept of objectivity from continuum mechanics, as it is also used in flow visualization, and in particular explain the corresponding notion of *objectively-determined observers* that we use in the main paper.

Objectivity and objective tensor fields

The basic intention of objectivity in continuum mechanics is that all possible, physically-realizable observers should *agree on objective properties or structures*. For example, they should agree on the location and properties of objectively-detected vortices. The standard definition of objectivity given by Truesdell and Noll [46, p.42] states the transformation rules that must be fulfilled by scalar fields, vector fields, and (second-order) tensor fields in Euclidean spaces, \mathbb{R}^2 and \mathbb{R}^3 , in order for these fields to be *objective*. These rules are, in fact, nothing more than the pushforwards/pullbacks (see Appendix D), as given by Eq. 30 and Eq. 31, of the frame change diffeomorphism, as given by Eq. 26. (Also see Marsden and Hughes [30, p.100], and Rautek et al. [39].)

More fundamental than the definition for specific fields, however, is that the concept of objectivity includes the fact that all observers agree on the motion of (Lagrangian) particles, in the sense of their *spatial location at any time*⁵. (It is important that this does not mean that they measure the same velocity field for this motion, since velocities depend on the specific reference frame that they are relative to. See below.) If we consider one specific particle, although the trajectory of the particle (its path line) will in general look different for every observer, e.g.,

⁵We note that our entire discussion, and the definition of objectivity, is concerned with *kinematics*, i.e., the description (and observation) of motions without considering the forces that cause these motions. The latter are a consideration in terms of *dynamics*, where the difference between inertial (non-rotating) reference frames and rotating reference frames is of crucial importance. However, for kinematical considerations, forces are irrelevant, and therefore in this context inertial frames are not special: In terms of kinematics, all physically-realizable, rotating or non-rotating (inertial), reference frames are the same class of reference frames and are treated equally. An example are hurricanes on Earth, which are fundamentally caused (in terms of forces) by the Earth’s rotation: They are a result of inertial (or “fictitious”) forces (mainly the Coriolis force) occurring in a rotating frame. However, the resulting motion of air, immersed particles, etc. comprising a hurricane can then be considered purely in terms of kinematics. That is, we can *observe* the hurricane’s motion from any physically-realizable, rotating or non-rotating, observer. Naturally, however, this does not change the hurricane’s motion, i.e., where particles are physically located at any one time.

straight for one observer, curved for another observer, see Fig. 5 (a,b), at any time t all observers will agree on where the particle is located.

Mathematically, to agree in this context means that where the particle is observed by one observer simply follows the observer transformation given by Eq. 26 to determine where another observer will observe the same particle. However, despite this transformation, the corresponding meaning is that both observers agree that the particle is at *the same* physical location. After all, it is physically the same particle, and as such it can only occupy one spatial location at any given time.

In coordinates, the transformation given by Eq. 26 transforms the same point (where the particle is located) from the coordinate system of one observer to that of the other observer. However, the underlying meaning is in fact coordinate-invariant, and Truesdell and Noll [46, p.42] also emphasize that the observer transformation given by Eq. 26 is independent of any particular choice of coordinate system.

Transformation of velocity fields

Corresponding to the motion of particles discussed above, any one specific observer can determine the velocity of a particle *with respect to its own reference frame*. This, however, implies that different moving observers will measure different velocities. Therefore, the input field \mathbf{v} to our framework will be a different field for each observer, depending on the reference frame relative to which it was measured or simulated.

Although velocity fields are not objective, the transformation rule for velocity fields (Eq. 32, see also the appendixes of Rautek et al. [39]) makes it easy to directly transform velocities given relative to one observer to velocities valid for another observer, such that the underlying motion is, again, *the same*. (The same is again meant in the sense of each particle occupying the same spatial location at any one time for all observers; in fact, this requirement is how the velocity transformation rule is derived in the first place.) This also implies that when the velocity transformation rule is used first, and *then* particle trajectories (path lines) are integrated by the other observer, the computed path lines will pass through the same spatial positions (at the corresponding time).

The velocity transformation rule (Eq. 32) is not the same as the transformation rule of an objective vector field (Eq. 30). (See Truesdell and Noll [46, p.42].) An important implication of this is that while the magnitude of each vector in an objective vector field does not change under transformation, the magnitudes (speeds) of velocity vectors do change (in Galilean relativity, different moving observers measure different speeds). The main difference between the two transformation rules is that in the velocity transformation the Killing field \mathbf{w} that describes the relative rigid motion between the two observers is subtracted out (Eq. 32), whereas in the objective transformation it is not (Eq. 30).

Objectively-determined velocity fields

We now make the crucial point that, despite two different moving observers measuring two different velocity fields for *the same* underlying motion (as above), the velocity field \mathbf{v} that each observer measures individually is nevertheless *determined objectively* by each observer. By this we simply mean the above: The underlying motion, which is observed and whose velocities are measured, is the same motion. However, the objectively-determined velocity field is *not* an objective vector field! For the input field \mathbf{v} being objectively determined is a rather obvious notion⁶, since all observers perceive the same underlying motion of particles to begin with. Where the notion of an objectively-determined velocity field becomes absolutely crucial, however, is when *an observer by itself determines a velocity field without being able to perceive a corresponding motion of particles or fluid parcels*. In our context, this concretely refers to computing a velocity field via mathematical optimization⁷. Such an optimization must result in an objectively-determined velocity field in order to be observer-indifferent.

⁶This property is usually not made explicit, and we are not aware of any standard term for this concept. We assume this is the case because velocity fields are usually measured for the motion of physically-observable objects (particles, fluid parcels), and the property of being objectively determined is trivially given.

⁷We note, however, that although maybe only computational methods are feasible in practice, such an optimization is not necessarily “non-physical.” At least in principle, we could achieve similar results by moving a physical grid

Another way to see this is that *if* two velocity fields $\mathbf{v}_1, \mathbf{v}_2$ (both measured relative to the same observer) are both objectively determined, *then* a vector field computed as their (pointwise) difference, i.e., a field

$$\mathbf{f} := \mathbf{v}_1 - \mathbf{v}_2, \quad (52)$$

is always an objective vector field according to the definition by Truesdell and Noll [46, p.42], corresponding to the pullback given by Eq. 30. The simple reason is that the Killing field of the observer transformation is the same for both velocity fields and thus cancels out when taking the difference between two (objectively-determined) velocity fields:

$$\begin{aligned} (\mathbf{v}_1^* - \mathbf{v}_2^*) &= \phi_t^*(\mathbf{v}_1 - \mathbf{w}) - \phi_t^*(\mathbf{v}_2 - \mathbf{w}), \\ &= \phi_t^*((\mathbf{v}_1 - \mathbf{w}) - (\mathbf{v}_2 - \mathbf{w})), \\ &= \phi_t^*(\mathbf{v}_1 - \mathbf{w} - \mathbf{v}_2 + \mathbf{w}), \\ &= \phi_t^*(\mathbf{v}_1 - \mathbf{v}_2). \end{aligned} \quad (53)$$

Thus, we have the transformation rule of Eq. 30: $\mathbf{f}^* = \phi_t^* \mathbf{f}$, and therefore \mathbf{f} is objective. However, the point about two velocity fields having to be objectively determined, in order for their *difference* to be objective, is crucial: *It is not true that the difference of any two velocity fields is objective*. This is quite natural: If two observers agree on the underlying motions (i.e., the respective velocity fields are determined objectively), then the difference vector field will be objective. Otherwise, it will not be objective, because they *do not agree* on the underlying motions.

Mathematically, the latter is a *violation of the velocity transformation rule* of a velocity field \mathbf{v} that is not objectively determined, meaning

$$\mathbf{v}^* \neq \phi_t^*(\mathbf{v} - \mathbf{w}). \quad (54)$$

Objectively-determined observer velocity fields

The same principle can now be applied to observer fields, which are velocity fields describing the motion of a field of observers, relative to any physically-realizable observer. As velocity fields, they transform with the standard velocity transformation rule, and are thus *not objective*. However, the crucial point is that an observer velocity field \mathbf{u} must be *determined objectively*, exactly as described above. This guarantees that the underlying motion (rigid or non-rigid) will be *the same*, independent of which physically-realizable observer actually determined the observer velocity field (which is thus relative to that observer).

The methods by Hadwiger et al. [18] and Rautek et al. [39] both guarantee this by performing an objective optimization, obtaining the observer velocity field \mathbf{u} as the unique minimizer of a functional that contains only objective quantities. Despite this apparent mixing of the concepts of “objective” vector fields and of “objectively-determined” velocity fields, this is exactly what is needed in this context: Since the arbitrary input field \mathbf{v} is determined objectively (see above), *and* the observer field \mathbf{u} is likewise determined objectively, guaranteeing that we have $\mathbf{u}^* = \phi_t^*(\mathbf{u} - \mathbf{w})$, for any possible observer \mathbf{w} , their difference

$$\mathbf{v} - \mathbf{u}, \quad (55)$$

is guaranteed to be an *objective* vector field. The method of Günther et al. [14] operates in the opposite way: It directly optimizes for an objective vector field $\bar{\mathbf{v}}$ (Eq. 20 in [14])⁸. But this means that the field

$$\mathbf{u} := \mathbf{v} - \bar{\mathbf{v}}, \quad (56)$$

is guaranteed to be an *objectively-determined* velocity field. Using either method, we can obtain exactly what we want: (1) An objectively-determined observer field \mathbf{u} , and (2) an objective vector field $(\mathbf{v} - \mathbf{u})$, as the difference between the input velocity field and the observer field.

of points connected by rigid rods (or a physical camera setup), and move this “reference frame” until we achieve the desired derivatives (e.g., minimal Eulerian time derivatives) measured relative to this physical reference frame motion.

⁸It is interesting to note that as an objective vector field, the field $\bar{\mathbf{v}}$ is not a velocity field, at least not in the reference frame of the input field \mathbf{v} . This also means that in that reference frame, it is incorrect to integrate the field $\bar{\mathbf{v}}$ to obtain path lines: There are no physical objects that are moving with velocity $\bar{\mathbf{v}}$ in that reference frame. (And if $\bar{\mathbf{v}}$ were a velocity field, it would transform as one.)

Objectively-determined, physically-realizable observers

The observer field \mathbf{u} above usually determines many different observers, and, in particular, it is typically (intentionally) not a Killing vector field. In order to obtain *physically-realizable* observers \mathbf{w} , we need to extract individual observers (Killing fields) from the overall velocity field \mathbf{u} , and confirm that the extracted observers are also *determined objectively*. Because we extract observers along path lines of the objectively-determined observer field \mathbf{u} (Sec. 3.3), which are Lagrangian and therefore objective, we only need to check the velocity gradients $\nabla \mathbf{u}$ along these path lines. However, this is a simple corollary from the above: The velocity gradients $\nabla \mathbf{u}$, including their extracted anti-symmetric parts $\nabla \mathbf{w}$ (Eq. 17 and Eq. 19), result from linear spatial operators. Thus, they simply transform as second-order tensors with the rule given by Eq. 34. Therefore, since the velocity field \mathbf{u} is determined objectively, the extracted velocity gradients $\nabla \mathbf{w}$ are determined objectively as well. Thus, both \mathbf{w} and $\nabla \mathbf{w}$ *along the path line* are determined objectively. However, now we can use the crucial Theorem 3.2 that states that knowing these two quantities on the path line determines the corresponding Killing field on the entire manifold M uniquely. Therefore, the entire extracted physically-realizable observer \mathbf{w} is determined objectively.

Thus, any observer extracted as in Sec. 3.3 will be an *objectively-determined* observer, *if* the velocity field \mathbf{u} is objectively determined.

Objectivity of averaged or interpolated observers

Averaging and interpolating a set of objectively-determined observers is a linear combination of observers. Thus, if all these observers are objectively determined, the corresponding averaged or linearly interpolated observer is also guaranteed to be objectively determined.

However, if we average or interpolate observers that are not (all) objectively determined, the corresponding average or linear interpolation will also not be objectively determined. An example for this case is using the lab frame observer, relative to which the input field is measured. The lab frame is usually not objectively determined (unless extracting a specific observer from an objectively-determined observer field \mathbf{u} results in the lab frame observer; by the lab frame observer this would be seen as a path line degenerated to a single critical point).

On the other hand, all observers resulting or extracted from an objectively-determined observer field \mathbf{u} (either because we use $\mathbf{u} := \mathbf{v}$, where \mathbf{v} is the objectively-determined input field, or because we have computed \mathbf{u} via objective optimization) can be averaged and/or interpolated, always resulting in an objectively-determined observer.

We note that the same concept is implicit in the original definition of LAVD by Haller et al. [21]. The region $U(t)$ that is used to compute the average vorticity must be a material region, which as such is objective. However, this approach is equivalent to averaging (the vorticity of) observers over the same material region $U(t)$, with the observers given by the observer field \mathbf{u} in the same region $U(t)$. The result is objectively determined when the field \mathbf{u} is objectively determined.

C COMPARING OBSERVERS

Expanding on comparing observers in Sec. 3.2, for the consistency of comparisons it is important to note that we have the following

Remark. *Because the metric tensor g_{ij} in Eq. 6 is defined via the integral of any given Lie algebra basis, the inner product of Killing fields obtained via Eq. 7 is invariant to the particular choice of basis.*

If this were not true, for a different choice of Lie algebra basis we would obtain different inner products. (The invariance above is the same as the invariance in any tensorial expression in tensor calculus.)

In terms of efficiency, we note that due to our expansion of any \mathbf{w}_1 and \mathbf{w}_2 with respect to basis Killing fields, for three-dimensional Lie algebras, the difference $d(\cdot, \cdot)$ can be computed as the component-wise subtraction of three-component vectors w_1^i and w_2^j , respectively, and the inner product is then simply computed via matrix multiplication with the 3×3 matrix g_{ij} . Moreover, because we choose orthogonal basis Killing fields, the matrix g_{ij} in fact is a diagonal matrix.

We now compute the specific metric tensor components g_{ij} for Killing fields in Euclidean and in spherical domains, respectively.

C.1 Comparing Observers in the Euclidean Plane

For the three basis Killing fields $\{\mathbf{e}_1, \mathbf{e}_2, \mathbf{e}_3\}$ for $M = \mathbb{R}^2$ given by Eq. 8, we obtain the corresponding metric tensor $g_{ij} := \langle \langle \mathbf{e}_i, \mathbf{e}_j \rangle \rangle$ as

$$g_{ij} = \begin{bmatrix} A & 0 & 0 \\ 0 & A & 0 \\ 0 & 0 & R \end{bmatrix}, \quad (57)$$

with $A = (x_b - x_a)(y_b - y_a)$, and $R = \frac{1}{3}A((x_b - \hat{x}_0)^2 + (y_b - \hat{y}_0)^2)$, where we again integrate over the rectangular domain $D = [x_a, x_b] \times [y_a, y_b] \subset \mathbb{R}^2$, with center point (\hat{x}_0, \hat{y}_0) . For a Killing field $\mathbf{w} = a\mathbf{e}_1 + b\mathbf{e}_2 + c\mathbf{e}_3$, we therefore compute its squared norm directly as

$$\|\mathbf{w}\|^2 = Aa^2 + Ab^2 + Rc^2. \quad (58)$$

The difference between two observers $\mathbf{w}_1 = a_1\mathbf{e}_1 + b_1\mathbf{e}_2 + c_1\mathbf{e}_3$ and $\mathbf{w}_2 = a_2\mathbf{e}_1 + b_2\mathbf{e}_2 + c_2\mathbf{e}_3$ is then quantified via

$$\langle \langle \mathbf{w}_1, \mathbf{w}_2 \rangle \rangle^2 = A(a_1 - a_2)^2 + A(b_1 - b_2)^2 + R(c_1 - c_2)^2. \quad (59)$$

We note that, since $A \neq R$, the relative weighting between linear and angular velocity, respectively, depends on the size of the domain.

Alternatively, it is also valid to *prescribe* any metric, by directly prescribing a matrix g_{ij} , e.g., a metric independent of the domain size.

C.2 Comparing Observers on the Sphere

For the three basis Killing fields $\{\mathbf{e}_1, \mathbf{e}_2, \mathbf{e}_3\}$ for $M = \mathbb{S}^2$ given by Eq. 11, we obtain the corresponding metric tensor $g_{ij} := \langle \langle \mathbf{e}_i, \mathbf{e}_j \rangle \rangle$ as

$$g_{ij} = \begin{bmatrix} R & 0 & 0 \\ 0 & R & 0 \\ 0 & 0 & R \end{bmatrix}, \quad (60)$$

with $R = \frac{8}{3}\pi$. For a Killing field $\mathbf{w} = a\mathbf{e}_1 + b\mathbf{e}_2 + c\mathbf{e}_3$, we therefore compute its squared norm directly as

$$\|\mathbf{w}\|^2 = Ra^2 + Rb^2 + Rc^2. \quad (61)$$

The difference between two observers $\mathbf{w}_1 = a_1\mathbf{e}_1 + b_1\mathbf{e}_2 + c_1\mathbf{e}_3$ and $\mathbf{w}_2 = a_2\mathbf{e}_1 + b_2\mathbf{e}_2 + c_2\mathbf{e}_3$ is then quantified via

$$\langle \langle \mathbf{w}_1, \mathbf{w}_2 \rangle \rangle^2 = R(a_1 - a_2)^2 + R(b_1 - b_2)^2 + R(c_1 - c_2)^2. \quad (62)$$

D DIFFERENTIALS AND PULLBACKS

We denote reference frame transformations by diffeomorphisms ϕ_t , with each map ϕ_t an isometry, from a manifold M to itself. Each map

$$\begin{aligned} \phi_t : M &\rightarrow M, \\ x &\mapsto \phi_t(x), \end{aligned} \quad (63)$$

induces a *differential* (or pushforward) $d\phi_t$ between tangent spaces on M (in fact on the tangent bundle TM). For each tangent space $T_x M$, i.e., the tangent space at the point $x \in M$, the differential is a linear map

$$\begin{aligned} (d\phi_t)_x : T_x M &\rightarrow T_{\phi_t(x)} M, \\ x &\mapsto (d\phi_t)_x(x). \end{aligned} \quad (64)$$

The differential maps vectors from points x to points $\phi_t(x)$.

In Sec. 5, for consistency and in order to avoid the frequent use of pushforwards of inverse diffeomorphisms ϕ_t^{-1} , we instead use the *pullback* ϕ_t^* , mapping “back” vectors from points $\phi_t(x)$ to points x by

$$(\phi_t^* \mathbf{x})_x := (d\phi_t^{-1})_{\phi_t(x)}(\mathbf{x}). \quad (65)$$

For second-order tensors \mathbf{T} , linearly mapping vectors to vectors, we in any case require the corresponding pullback ϕ_t^* of \mathbf{T} , defined by

$$\begin{aligned} (\phi_t^* \mathbf{T})_x : T_x M &\rightarrow T_x M, \\ x &\mapsto (\phi_t^* \mathbf{T})_x(\mathbf{x}) := d\phi_t^{-1}(\mathbf{T}(d\phi_t(\mathbf{x}))). \end{aligned} \quad (66)$$

While pullbacks in general are defined for smooth maps that need not be diffeomorphisms, the above definitions require the map ϕ_t to be a diffeomorphism (guaranteed to have an inverse) to allow mapping back vectors in the inverse direction ϕ_t^{-1} , which in our context is fulfilled.

E OBSERVER TRANSFORMATION ON THE SPHERE

We now concretely give the reference frame transformation, described in general and for the Euclidean plane in Sec. 5.1, for the sphere.

Frame change diffeomorphism (isometry) on the sphere

The time-dependent isometry ϕ_t for frame transformation on the sphere, corresponding to a rigid motion (i.e., rotation) of the sphere, is given by

$$\phi_t(x) = \mathbf{r}^{-1}(\mathbf{R}(t) \mathbf{r}(x)). \quad (67)$$

Here, $\mathbf{r}(x)$ is a 3D vector pointing from the center of the sphere to the point x on the sphere, embedded in \mathbb{R}^3 , $\mathbf{R}(t)$ is the total integrated 3×3 rotation matrix giving the rigid transformation of the sphere at time t , and $\mathbf{r}^{-1}(\cdot)$ denotes the inverse of $\mathbf{r}(\cdot)$ interpreted as a function, mapping “back” a vector pointing from the center of the sphere to the point $\phi_t(x)$ embedded in \mathbb{R}^3 , to the “intrinsic” point $\phi_t(x)$ on the sphere.

Pullback on the sphere

The corresponding pullback ϕ_t^* of a vector field \mathbf{x} on the sphere is

$$\phi_t^* \mathbf{x} = (\mathbf{B}^*)' \mathbf{R}^T(t) \mathbf{B} \mathbf{x}. \quad (68)$$

The pullback ϕ_t^* of a second-order tensor field \mathbf{T} on the sphere is

$$\phi_t^* \mathbf{T} = (\mathbf{B}^*)' \mathbf{R}^T(t) \mathbf{B} \mathbf{T} \mathbf{B}' \mathbf{R}(t) \mathbf{B}^*. \quad (69)$$

The $\mathbf{R}(t)$ are the same rotation matrices as above. The 3×2 matrices \mathbf{B} , \mathbf{B}^* map vectors \mathbf{x} , at $\phi_t(x)$, and \mathbf{x}^* , at x , respectively, from two components referred to tangent space bases embedded in \mathbb{R}^3 , $\{\mathbf{b}_1, \mathbf{b}_2\}$, at $\phi_t(x)$, and $\{\mathbf{b}_1^*, \mathbf{b}_2^*\}$, at x , respectively, to their embedding in \mathbb{R}^3 . The corresponding 2×3 matrices \mathbf{B}' , $(\mathbf{B}^*)'$ perform the “inverse” operation, mapping 3D vectors, tangent to the sphere, back from three to two components, again referred to the bases $\{\mathbf{b}_1, \mathbf{b}_2\}$, $\{\mathbf{b}_1^*, \mathbf{b}_2^*\}$, respectively.

In case the vectors are given embedded in \mathbb{R}^3 , instead of as intrinsic 2D vectors, and the tensors \mathbf{T} are likewise given embedded in 3D, the above matrices \mathbf{B} , \mathbf{B}^* , \mathbf{B}' , $(\mathbf{B}^*)'$ simply become identity matrices.

F OBSERVED TIME DERIVATIVES

The observed time derivative, which was originally given by Hadwiger et al. [18] for flat (Euclidean) spaces (in 2D and 3D), but is also well-defined for curved spaces [39], is given by the differential operator

$$\frac{\mathcal{D}}{\mathcal{D}t} := \frac{\partial}{\partial t} + \mathcal{L}_{\mathbf{u}}. \quad (70)$$

This operator gives the derivative of a time-dependent tensor field with respect to the flow of a given vector field, here denoted by \mathbf{u} , where, crucially, the semantic meaning of the field \mathbf{u} is that of an observer field [18, 39], i.e., it describes the motion of (one to many) observers.

The operator \mathcal{L} used above denotes the (autonomous) Lie derivative, which is standard in differential geometry and mathematical physics [12], measuring the rate of change of a tensor (including vector) field with respect to the flow of a given vector field. Here, this is the flow of the observer velocity field \mathbf{u} , which we denote by writing $\mathcal{L}_{\mathbf{u}}$.

For the specific case of a physically-realizable observer, given by a Killing field \mathbf{w} , we use the same operator by simply using the field \mathbf{w} ,

$$\frac{\mathcal{D}}{\mathcal{D}t} := \frac{\partial}{\partial t} + \mathcal{L}_{\mathbf{w}}. \quad (71)$$

We can obtain the time derivative of any input flow field \mathbf{v} , as observed by the observer determined by the Killing field \mathbf{w} , by applying this operator to the relative velocity field $(\mathbf{v} - \mathbf{w})$, i.e., we compute

$$\frac{\mathcal{D}}{\mathcal{D}t}(\mathbf{v} - \mathbf{w}) = \frac{\partial \mathbf{v}}{\partial t} - \frac{\partial \mathbf{w}}{\partial t} + \nabla \mathbf{v}(\mathbf{w}) - \nabla \mathbf{w}(\mathbf{v}). \quad (72)$$

On the right-hand side, we have simply expanded the (autonomous) Lie derivative, which for vector fields is identical to the differential-geometric Lie bracket, as given above (Eq. 49). See previous work [18, 39] for more details on and usage of observed time derivatives, in particular for the objective optimization of observer fields, where the a priori unknown field \mathbf{u} is computed such that $(\mathcal{D}/\mathcal{D}t)(\mathbf{v} - \mathbf{u})$ is minimized, making the observed field “as steady as possible.”

G OBSERVED ACCELERATION

The acceleration of a massless particle in a velocity field \mathbf{v} is

$$\mathbf{a} = \nabla \mathbf{v}(\mathbf{v}) + \frac{\partial \mathbf{v}}{\partial t}. \quad (73)$$

By substituting observed quantities in this definition, we obtain the *observed acceleration*, as the acceleration relative to the observer \mathbf{w} , as

$$\begin{aligned} \mathbf{a}^* &= \nabla \mathbf{v}^*(\mathbf{v}^*) + \frac{\partial \mathbf{v}^*}{\partial t}, \\ &= \phi_t^* \left(\nabla(\mathbf{v} - \mathbf{w})(\mathbf{v} - \mathbf{w}) + \frac{\mathcal{D}}{\mathcal{D}t}(\mathbf{v} - \mathbf{w}) \right). \end{aligned} \quad (74)$$

Inserting Eq. 73, we can compute the observed acceleration \mathbf{a}^* directly from the acceleration \mathbf{a} and the fields \mathbf{v} and \mathbf{w} as

$$\mathbf{a}^* = \phi_t^* \left(\mathbf{a} - \frac{\partial \mathbf{w}}{\partial t} - 2\nabla \mathbf{w}(\mathbf{v}) + \nabla \mathbf{w}(\mathbf{w}) \right). \quad (75)$$

We note that, in fact, the term $2\nabla \mathbf{w}(\mathbf{v})$ corresponds to what is known as the *Coriolis acceleration* $2\boldsymbol{\Omega}\mathbf{v}$, and the term $\nabla \mathbf{w}(\mathbf{w})$ corresponds to what is known as the *centripetal acceleration* $\boldsymbol{\Omega}\mathbf{w}$, of a rotating reference frame, with angular velocity of the rotating frame $\boldsymbol{\Omega} = \nabla \mathbf{w}$.

In terms of the observer \mathbf{w} as $t \mapsto (a(t), b(t), c(t))$, as for the other quantities above we can insert the terms given in Eq. 25 into Eq. 75.

H DATA SETS

Data set sizes used for the evaluation of our method are given in Table 2.

Table 2. Data set sizes used for evaluation.

data set	size	time steps
Cylinder Flow with von Kármán vortex street (simulated)	640×80	1,000
Heated cylinder with Boussinesq approximation (simulated)	150×450	800
Beads problem (analytic)	128×128	512
Divergence free beads flow (analytic)	128×128	256
Four rotating centers (analytic)	128×128	256
Cylinder flow Jung, Tel and Ziemniak (analytic)	450×200	500
Bickley jet (analytic)	300×60	300
Vortex on sphere triangle mesh (analytic)	7,608 triangles	64

I PERFORMANCE ANALYSIS

We separate the computation of observed path lines into three parts. First, the computation of a set of path lines in the lab frame is performed in parallel on the CPU, where each CPU core integrates one path line. We upload the resulting vertex positions to a buffer on the GPU. Second, when an observer is specified we compute the time dependent diffeomorphism using numerical integration on the CPU (Eq. 29). We upload the resulting array of transformation matrices $\mathbf{Q}(t)$, for each time sample $t = t_i$ to the GPU. Lastly, the transformation of the path lines (Eq. 40) is implemented on the GPU. Each vertex is transformed by the corresponding transformation matrix in the vertex shader.

The separation of the computation into these three parts allows us to independently update the set of path lines, as well as the observer, without the need to recompute the integration of the observed path lines.

We have run performance tests for different data sets, numbers of path lines, and integration step sizes, on a workstation with two Intel Xeon 6230R processors with a total of 52 CPU cores, and an NVIDIA GeForce RTX 3090 GPU.

Table 3 shows performance numbers that were averaged over 1,000 runs of path line integrations. The number of integration steps that are required to reach high-quality visualizations strongly depends on the data set. We typically use two to ten samples for each time step of a data set. Table 3 shows that the performance mostly depends on

the number of vertices generated by the numerical integration. When integrating enough path lines in parallel we achieve more than 15 million vertices per second.

Table 4 shows performance numbers that were averaged over 1,000 runs for the computation of the transformation matrices used for the diffeomorphism. Since we compute $\nabla \mathbf{w}$ for each time step along the observer world line, the performance depends on the number of time steps of the data set as well as the number of samples taken along the observer world line. Table 4 shows that the number of samples has less influence than the number of time steps. We found in all our experiments that computing the transformation matrices for the diffeomorphism with a high number of samples and transferring the data to the GPU takes less than 100 ms.

The performance impact of the transformation in the vertex shader is only one additional matrix-vector multiplication per vertex. We measured the frame rate of our rendering algorithm and found that we get 20–30 frames per second for conventional path line rendering as well as observed path line rendering.

Table 3. Pathline integration performance.

data set	number of pathlines	time [ms]	throughput [vertices/s] in millions
Four centers	64	26	15
	128	48	17
	256	83	19
	512	154	21
	1,024	238	27
Heated cylinder (Boussinesq)	64	23	14
	128	40	16
	256	76	17
	512	150	17
	1,024	293	17

Table 4. Diffeomorphism computation performance.

data set	number of samples	time [ms]	throughput [samples / s] in thousands
Four centers	6.28×10^1	5	12
	6.28×10^2	6	100
	6.28×10^3	12	509
	6.28×10^4	87	723
Heated cylinder (Boussinesq)	5×10^1	11	4
	5×10^2	13	38
	5×10^3	21	234
	5×10^4	82	609